# Bio-inspired coating for feed spacers

## Managing biofouling and controlling biofilm populations in seawater RO systems

Venkidusamy, Krishnaveni; Pulido-Beltran, Laura; Buijs, Paulus J.; Miller, Daniel J.; Vrouwenvelder, Johannes S.; Farhat, Nadia M.

**DOI**
10.1016/j.memsci.2025.123809

**Publication date**
2025

**Document Version**
Final published version

**Published in**
Journal of Membrane Science

**Citation (APA)**
Venkidusamy, K., Pulido-Beltran, L., Buijs, P. J., Miller, D. J., Vrouwenvelder, J. S., & Farhat, N. M. (2025). Bio-inspired coating for feed spacers: Managing biofouling and controlling biofilm populations in seawater RO systems. *Journal of Membrane Science*, *722*, Article 123809. https://doi.org/10.1016/j.memsci.2025.123809

Journal of Membrane Science 722 (2025) 123809

Contents lists available at ScienceDirect

Journal of Membrane Science

journal homepage: www.elsevier.com/locate/memsci

# Bio-inspired coating for feed spacers: Managing biofouling and controlling biofilm populations in seawater RO systems

Krishnaveni Venkidusamy [a,*], Laura Pulido-Beltran [a], Paulus J. Buijs [a], Daniel J. Miller [c], Johannes S. Vrouwenvelder [a,b,d], Nadia M. Farhat [a,**]

[a] Water Desalination and Reuse Center (WDRC), King Abdullah University of Science and Technology (KAUST), Thuwal, 23955-6900, Saudi Arabia
[b] Environmental Science and Engineering Program, Biological and Environmental Science and Engineering (BESE) Division, King Abdullah University of Science and Technology (KAUST), Thuwal, 23955-6900, Saudi Arabia
[c] Chemical Sciences Division, Lawrence Berkeley National Laboratory, Berkeley, CA, 94702, USA
[d] Delft University of Technology, Faculty of Applied Sciences, Department of Biotechnology, Van der Maasweg 9, 2629 HZ, Delft, the Netherlands

ARTICLE INFO

*Keywords:*
Seawater reverse osmosis systems
Eco-innovative antibiofouling coating
Biofouling mitigation
Polydopamine-sodium periodate
Citric acid blended tannic acid (cTA)
*In-situ* and E*x-situ* coating

ABSTRACT

This study addresses the pervasive challenge of biofouling in seawater desalination systems, which compromises membrane performance and longevity, by introducing a multifunctional PDA-SP-cTA coating. This bio-inspired coating effectively mitigates biofouling in seawater reverse osmosis systems without requiring biocide. The coating is applied to both hydrophilic polyamide membranes and hydrophobic polypropylene feed spacers through *in-situ* and *ex-situ* polymer deposition methods, involving a single-step process with polydopamine and sodium-periodate, followed by surface tailoring with citric acid-blended tannic acid. Extensive surface characterization, primarily conducted on polypropylene feed spacers, confirms coating deposition. Antibiofouling properties are evaluated through long-term biofouling tests simulating industrial conditions. The findings demonstrate that the *ex-situ* applied coating significantly reduces relative feed channel pressure drop increase due to biofilm growth by 75 % and lowers biomass accumulation (88 % total cell counts, 70 % adenosine-triphosphate, 91 % carbohydrates, and 69 % proteins). The coating inhibits the colonization of biofouling-causing bacterial genus *Alteromonas*, drastically decreases active bacterial gene copy numbers, and alters microbial composition, leading to reduced biofilm viability and loosely attached biofilms that could enhance cleaning efficiency. This comprehensive study encompasses the entire process from the strategic selection and systematic characterization of the coating to extensive biofouling tests and stability assessments offering a holistic solution to combat biofouling without biocides. With demonstrated durability and stability across various pH conditions over time, this coating could be a widely applicable and scalable solution for biofouling mitigation in diverse industrial contexts.

## 1. Introduction

Membrane-based desalination plays a pivotal role in addressing freshwater scarcity by delivering high-quality drinking water. However, membrane fouling, particularly biofouling, poses a significant challenge to the widespread adoption of this technology [1]. Biofouling, defined as the undesired accumulation, growth, and metabolic activities of microorganisms including bacteria on membrane surfaces often leads to unacceptable performance declines in desalination systems [2]. Microbial cells and organic macromolecules from water sources form conditioning films on membrane surfaces, facilitating robust biofilm development [3]. These biofilms provide microorganisms with enhanced nutrient access and antimicrobial resistance, making them resilient to the rigorous conditions of membrane filtration [4]. Biofouling increases osmotic pressure, causes pressure drops across membrane modules, and significantly deteriorates system performance [5]. Moreover, biofilm proliferation results in the release of extracellular polymeric substances (EPS), which bind inorganic ions to membrane surfaces, further exacerbating fouling and operational inefficiencies. Effective control of biofouling is therefore essential for the sustainable

* Corresponding author.
** Corresponding author.
*E-mail addresses:* krishnaveni.venkidusamy@mymail.unisa.edu.au (K. Venkidusamy), nadia.farhat@kaust.edu.sa (N.M. Farhat).

https://doi.org/10.1016/j.memsci.2025.123809
Received 1 November 2024; Received in revised form 28 January 2025; Accepted 2 February 2025
Available online 6 February 2025

and efficient operation of reverse osmosis (RO) desalination plants.

Desalination facilities rely on chemical cleaning to manage biofouling, but these methods are often ineffective and environmentally harmful [1,6]. Consequently, research has shifted toward sustainable antibiofouling (ABF) strategies, including enhanced pretreatment, improved cleaning programs, and innovative surface modifications [7]. Among these, eco-friendly coatings have shown great promise. Recent studies highlight topological strategies, like sharkskin-patterned membranes and synergistic chemical-topological modifications, for eco-friendly biofouling reduction [8,9]. Building on these advancements, mussel-inspired polydopamine (PDA) coatings offer a versatile platform for priming hydrophobic surfaces like polypropylene (PP), enabling the deposition of additional functional layers [10]. However, PDA alone offers limited long-term biofouling resistance under dynamic conditions [11], necessitating enhancements with antimicrobial agents such as peptides [12], antibiotics [13], and metal ions [14], which balance effectiveness with environmental sustainability despite practical trade-offs [15,16]. Addressing these challenges, our research focuses on scalable, eco-friendly ABF coatings that minimize biocide usage while effectively targeting biofouling in membranes and spacer-filled channels [17,18]. Advances in non-toxic oxidants, like sodium metaperiodate (SP), have enabled superhydrophilic PDA coatings that significantly reduce protein fouling and microbial attachment, mimicking natural self-cleaning processes [19,20]. Additionally, Tannic acid (TA), known for its hydrophilic, bactericidal, and self-cleaning properties, further enhances coating functionality and sustainability [21–24]. Citric acid is also used as a functional antimicrobial additive that enhances the coating's stability, redox functionality, and overall antibiofouling efficacy [24]. This synergy effectively mitigates biofouling across diverse system components.

To develop environmentally friendly antibiofouling (ABF) coatings for seawater desalination, we adopted a novel two-step approach combining polydopamine-sodium metaperiodate (PDA-SP) and citric acid-blended tannic acid (cTA). This innovative method, tailored for polypropylene (PP) feed spacers, employs PDA priming under slightly acidic conditions (pH 5.0) to enhance adhesion and coating stability. Subsequently, SP and cTA are layered to create a more hydrophilic surface that effectively reduces biofoulant adhesion, minimizes biofilm formation, and prevents protein denaturation [19]. Notably, this integration of SP and cTA with PDA for application on PP feed spacers represents a novel approach not previously documented. While PDA and TA share properties like adhesion and hydrophilicity, their roles in the PDA-SP-cTA system are distinct yet complementary: PDA promotes adhesion to hydrophobic PP surfaces and provides reactive catechol groups for SP and cTA deposition, ensuring stability and functionality. SP degrades polysaccharide adhesins critical for biofilm formation by oxidizing hydroxyl carbons, resulting in C–C bond cleavage [25], while the addition of tannic acid and citric acid at pH 4.0 enhances stability, redox functionality, and antibiofouling efficacy [26]. This coating, applied via both *in-situ* and *ex-situ* methods, demonstrates substrate-independent effectiveness on both hydrophobic PP and hydrophilic PA membranes. Systematic evaluations of the PDA-SP-cTA coating's biofouling control were conducted in real seawater desalination scenarios using membrane fouling simulators (MFS) with ultrafiltration (UF) pretreated seawater from KAUST's Tahliah Almiah plant. While biofouling control research has traditionally focused on membrane modification, significant biofouling occurs within spacer-filled channels [27], heavily influenced by the surface characteristics and configurations of the feed spacers [28]. Our study specifically evaluates the coating's performance in non-permeation mode, isolating its impact on feed spacer biofouling without confounding variables from membrane permeation. Continuous monitoring of feed channel pressure, biomass development, and post-autopsy quantification confirmed its effectiveness. Advanced techniques like nanopore-based sequencing (Oxford Nanopore Technologies) and reverse transcription-quantitative polymerase chain reaction (RT-qPCR) were employed to evaluate the PDA-SP-cTA coating's impact on naturally formed multispecies biofilms in seawater desalination systems. Overall, the study highlights the PDA-SP-cTA coating's effectiveness in controlling biofouling, with a focus on practical outcomes in both *in-situ* and *ex-situ* conditions, rather than the detailed mechanistic interactions.

Our research introduces a novel PDA-SP-cTA combination, advancing long-term biofouling control in seawater desalination with a targeted and effective antibiofouling solution. Unlike prior studies focused on short-term effects with standard antimicrobials [11,19,24,29–33], this innovative approach demonstrates superior long-term efficacy and transcends traditional limitations. Our comprehensive study encompasses strategic material selection, systematic characterization, extensive biofouling tests, and stability assessments, delivering an integrated solution with minimal environmental impact. Using both in-situ and *ex-situ* methods, this scalable surface modification strategy adapts to diverse materials and geometries, advancing bio-inspired antibiofouling technologies and enhancing current applications.

## 2. Materials and methods

### 2.1. Materials and reagents

Commercial polyamide (PA) membranes and polypropylene (PP) feed spacers were procured from DuPont, USA (Dupont SW30 HRLE 4040). Chemicals and reagents, including sodium metaperiodate, anhydrous sodium acetate, glacial acetic acid, tris(hydroxymethyl) aminomethane, sodium chloride, citric acid, hydrochloric acid, tannic acid, ethanol, isopropanol, sodium dihydrogen phosphate, sodium nitrate, phosphate-buffered saline (PBS, pH ~ 7.0), formaldehyde, RNase, and RNAlater, were sourced from Sigma-Aldrich (St. Louis, MO, USA). Dopamine hydrochloride (99 %) was obtained from Alfa Aesar. Sodium hydroxide and nutrient broth were procured from Fisher Scientific (Pittsburgh, PA, USA). A sodium acetate buffer, used extensively in the modifications, was prepared by dissolving sodium acetate and acetic acid in deionized water, adjusting the pH to 5.0. The LIVE/DEAD BacLight™ Bacterial Viability Kit was sourced from Thermo Fisher (Waltham, MA, USA). For surface characterization studies, we employed 3D-printed polypropylene (PP) strips as surrogates for the diamond-shaped PP feed spacers typically found in seawater reverse osmosis systems. This approach, driven by the precise replication capabilities of 3D printing, enabled accurate emulation of the complex geometries and surface characteristics of actual feed spacers. Using these PP strips ensured consistency and reproducibility in our measurements, which are crucial for assessing the efficacy of our bio-inspired coatings. The choice of polypropylene, due to its chemical stability and similarity to commercial spacers, ensures that our findings on hydrophilicity, charge distribution, and microbial adhesion are directly applicable to real-world scenarios. This method effectively addressed the challenges associated with large pore sizes, which can complicate detailed assessments in traditional setups. Ultrapure water from Millipore MilliQ IQ 7000 was used for solution preparation. All chemicals were used without further purification and met commercial analytical grade standards.

### 2.2. Surface modification of membranes and feed spacers

Before surface modification, membrane coupons were rinsed in an aqueous IPA solution (25 %) for 10 min and stored in deionized water (DI) water for at least 24 h. All PP materials underwent ultrasonic cleaning in isopropanol and DI water for 15 min and were dried under nitrogen. In this study, a two-step process was followed to modify membranes and feed spacers: (i) Initially, the membranes and feed spacers were surface-modified by single-step deposition of a polydopamine (PDA) coating. This process involved the chemical oxidation of sodium metaperiodate (SP) under mildly acidic conditions (pH 5.0), as detailed by Ponzio et al. [19]. The resulting PDA-coated spacers and membranes were denoted as PDA-SP. (ii) In the second step, tannic acid

(TA) was coated onto the PDA SP-coated membranes and spacers, employing citric acid (CA) as a functional additive. The resulting membranes and feed spacers were labeled as PDA-SP-cTA. The coating process was carried out through either *in-situ* synchronous assembly, involving the pumping of polymerized solutions through the membrane module, or an *ex-situ* dip-coating process under shaking conditions at room temperature. The protocol for *in-situ* and *ex-situ* modification of membranes and spacers was adapted and modified from previous studies [11,19,20], as schematically indicated in Fig. 1. For comprehensive details on the *in-situ* and *ex-situ* modification processes, and the associated experimental protocols, please refer to the Supplementary Information section.

### 2.3. Surface characterization

Surface properties known to influence microbial deposition were characterized for each functionalized surface and compared to unmodified controls using various surface characterization techniques [34]. For further insights into the specifics of the surface characterization techniques and measurements used in this study, please refer to the Supplementary Information.

### 2.4. Coating stability and durability assessment

To evaluate the stability and durability of the PDA-SP-cTA coating, modified samples were subjected to immersion tests in solutions with pH values ranging from 1 (highly acidic) to 13 (highly alkaline). These samples were continuously agitated at 100 rpm at room temperature for 30 days. Stability assessments were conducted through visual observations and IR spectroscopy on days 1, 3, 7, and 30 across the entire pH spectrum. Adjustments to the pH were made as necessary using 0.1 M hydrochloric acid and 0.1 M sodium hydroxide in deionized (Milli-Q) water. After incubation, the visual observations and IR spectra of the samples before and after the incubation period were compared. All samples were thoroughly rinsed with Milli-Q water and dried under nitrogen before measurements.

### 2.5. Antibiofouling performance assessments

#### 2.5.1. MFS experimental setup

To evaluate the antibiofouling effectiveness of the coatings, long-term biofouling tests were conducted within a membrane fouling simulator (MFS) [35]. These tests were performed without permeate production used ultrafiltration-pretreated seawater as feed water with nutrient dosing under conditions that closely mimic those encountered in industrial installations [36]. Despite the effectiveness of ultrafiltration in removing larger bacteria, smaller microorganisms such as *ultramicrobacteria* and viruses, as well as soluble microbial products (SMPs), can still pass through and initiate biofilm formation. Additionally, variations in operational conditions and cleaning regimes may increase the susceptibility of UF systems to biofouling. The MFS, a lab-scale flow cell representative of spiral-wound membrane modules, comprised essential components including a reverse osmosis polyamide (PA) membrane, polypropylene (PP) feed, and permeate channel spacers [37]. The experimental setup included key elements such as an MFS with a feed water pump, a biodegradable nutrient dosage pump, a permeate flow meter, a back pressure valve, and a feed channel differential pressure sensor. The PA membrane in the MFS had active permeation area dimensions of 20 cm × 4 cm. A 34 mil (864 μm) thick feed spacer and a 250 μm thick permeate spacer were used at the feed and permeate channels. In this study, we chose to operate the MFS without permeate production, aligning with our specific focus on evaluating the antibiofouling properties of coatings on feed spacers rather than overall membrane performance. Supporting this approach, findings from Vrouwenvelder et al. (2009) indicated that permeate production does not significantly impact biofouling on spiral-wound membranes, especially where ultrafiltration or similar pretreatments are used [27,38]. The research also emphasizes that the predominant biofouling effect in full-scale RO systems is the increased pressure drop within feed spacer channels rather than direct impacts on permeability or rejection rates. This focus on non-permeation mode in our study ensures our results directly address feed spacer biofouling, which is a critical factor in the operational stability and maintenance needs of seawater RO systems. These findings validate our methodological choice, demonstrating that the impact of our antibiofouling coatings on biofouling mitigation can be accurately assessed without the confounding effects of permeate flow, thus offering clear insights into their efficacy in operational RO environments.

#### 2.5.2. Operating conditions

Eighteen fully independent MFS units were run in parallel in cross-flow at a constant pressure of 2 bar and with no permeate production for five days to evaluate the antibiofouling effectiveness of the coating (Table 1). The MFS units were operated at a flow rate of 20.0 $L \cdot h^{-1}$,

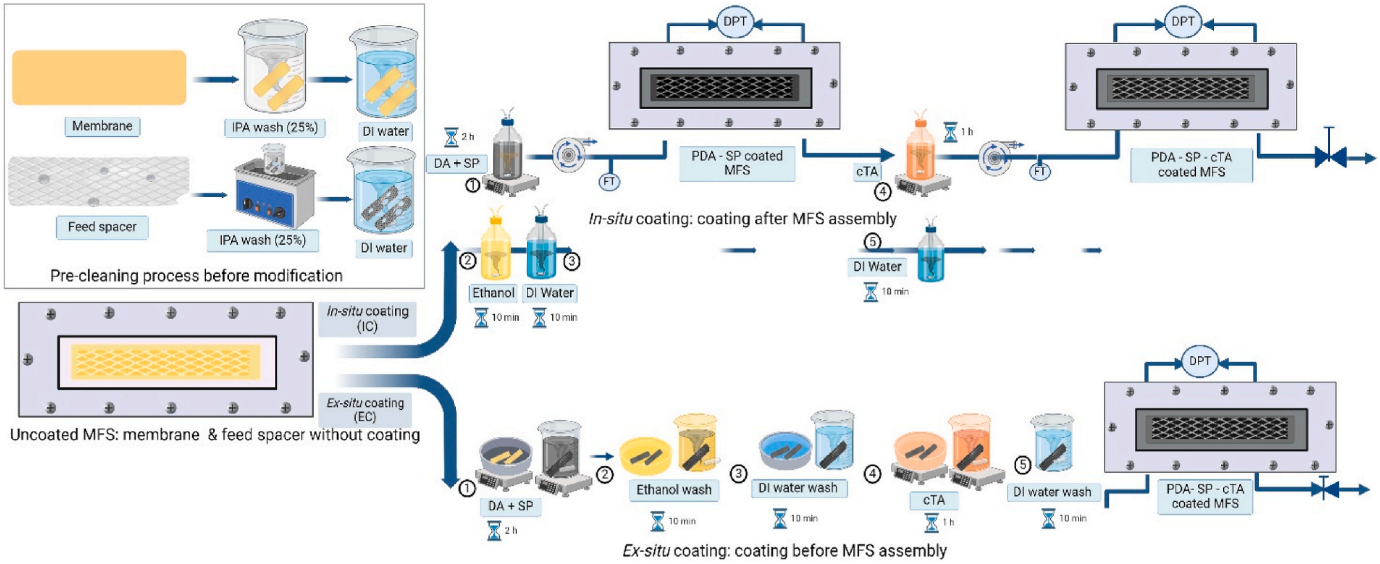


**Fig. 1.** Schematic of the *in-situ* vs. *ex-situ* coating processes in Membrane Fouling Simulators (MFS), highlighting key stages.

**Table 1**
Experimental conditions and descriptions used in the study.

| Experimental Conditions | MFS Code | Substrate Dosage | Coating Methods | Remarks |
|---|---|---|---|---|
| E1: Uncoated | UC | Yes | No coating | Positive control: biofouling is expected |
| E2: Uncoated control | UC-S | No | No coating | Negative control: biofouling is not expected |
| E3: *In-situ* coating | IC | Yes | Coat after MFS assembly | Evaluating the impact of *in-situ* polymer coating on biofouling |
| E4: *In-situ* coating control | IC-S | No | Coat after MFS assembly | Control: does polymer coating itself contribute to biofouling |
| E5: *Ex-situ* coating | EC | Yes | Coat before MFS assembly | Evaluating the impact of *ex-situ* polymer coating on biofouling |
| E6: *Ex-situ* coating control | EC-S | No | Coat before MFS assembly | Control: does polymer coating itself contribute to biofouling |

which is equivalent to a linear flow velocity of 0.196 $m{\cdot}s^{-1}$. To accelerate biofilm development, biodegradable nutrients in a mass ratio of 100:20:10 with a final carbon concentration of 100 μg C $L^{-1}$ were introduced into the feed water of the MFS units designated for the positive controls and coating test groups. The nutrient solution contained sodium acetate, sodium nitrate, and sodium phosphate. Conversely, negative control groups received no nutrient dosage. To prevent bacterial growth in the nutrient stock solution, we adjusted the pH to 11 using a 1 M NaOH solution. The amount of substrate solution added to the feed water was minimal (0.03 L $h^{-1}$) compared to the feed water flow rate (20.0 $L{\cdot}h^{-1}$). Consequently, the elevated pH of the substrate solution had no impact on the feed water pH, which remained at 7.8 [37]. All experiments were conducted across three independent replicate MFSs, and the figures present the average values along with the corresponding standard deviations obtained from the three runs.

### 2.5.3. Biofouling monitoring

*2.5.3.1. System performance parameters: evaluation of feed channel pressure drop.* Pressure drop measurements were recorded along the length of the MFS as an indicator of RO biofouling, as feed channel pressure drop (FCP) was shown to be the earliest and most strongly impacted performance indicator [38]. The FCP was measured as a relative pressure drop (RPD) increase and a 300 % RPD increase was used as a threshold to stop the positive control MFSs that were fed with nutrients. The pressure drop for each MFS was normalized to the initial starting pressure drop of 20 ± 3 mbar.

*2.5.3.2. Biomass quantification and characterization*

*2.5.3.2.1. Optical coherence tomography (OCT).* The effect of coatings on biofilm spatial distribution was investigated using real-time optical coherence tomography (OCT) with a Thorlabs Ganymede OCT System. This OCT system employs a central light source at 930 nm and a refractive index of 1.3. It is equipped with a 5 × telecentric scan lens (Thorlabs LSM03BB) that allows a maximum scanning area of 100 $mm^2$. OCT scans were acquired at a 36 kHz A-scan rate with a resolution of 1000 pixels × 1000 pixels, which corresponds to a 4.0 mm × 4.0 mm membrane surface). 2D cross-sectional OCT scans were regularly captured at the inlet, middle, and outlet of each MFS. For visualizing the biofouling layer on the membrane surface, Thorlabs SD-OCT system software was used. Subsequent analysis of biofilm structure, thickness, and volume was conducted based on the OCT scans. The OCT images were processed with Fiji Image J software (National Institutes of Health, USA). The biofilm thickness was estimated by averaging multiple local thicknesses from different biofilm locations. The images shown in this study were representative of all the images analyzed.

*2.5.3.2.2. Extraction of biofilm from the membrane surface.* At the end of the experiments, each MFS was stopped and autopsied for biomass characterization. Membranes and feed spacers were removed from the MFS and cut into equal-sized coupons (inlet, middle and outlet). To separate the biomass from the membranes and feed spacers, the coupons were immersed in the respective extraction solutions. Specifically, for ATP assessment, the biomass was extracted using autoclaved tap water; for FCM and TOC analyses, Milli-Q water was utilized; and for EPS examination, the biomass was separated using PBS buffer. The coupons were then subjected to vortex mixing (IKA Vortex 2) for 2 min, followed by 5 min of bath sonication (Branson, Model 5510MTH). The extracted biomass suspensions were then subjected to individual assessments, including DNA and RNA evaluations. For detailed methodologies regarding flow cytometry [39,40], ATP [41], TOC analyses, and EPS characterization [42], please refer to the Supplementary Information.

*2.5.3.2.3. DNA, RNA extraction, cDNA synthesis, and sequencing.* Microbial genomic DNA was extracted from 4 × 4 $cm^2$ coupons of the biofouled membrane and spacer using the FastDNA Spin Kit for Soil (MP Biomedicals, USA), following the manufacturer's protocol. The concentration of DNA was determined using the Qubit dsDNA HS/BR Assay Kit (Thermo Fisher Scientific, USA). For RNA extraction, the standard protocol of the RNeasy PowerMicrobiome Kit (Qiagen, Germany) was employed, and the concentration of RNA was measured with the Qubit RNA HS/BR Assay kit (Thermo Fisher Scientific, USA). To facilitate downstream applications, we conducted reverse transcription to cDNA using the SuperScript IV Reverse Transcriptase kit, following the manufacturer's instructions (Thermo Fisher Scientific, USA). To ensure the removal of all DNA in the RNA samples, DNase Max Kit (Qiagen, Germany) treatment was performed. Subsequently, RNA quality was assessed using RNA Screen Tape (Agilent, USA) and the Qubit RNA HS/BR Assay Kit (Thermo Fisher Scientific, USA).

*Rationale for using advanced RNA-based RT-qPCR molecular techniques*

In this study, advanced molecular techniques such as RNA-based 16S rRNA amplicon sequencing and RT-qPCR were employed to analyze microbial colonization and activity. These methods were selected for their superior sensitivity and ability to provide detailed insights into microbial activity, gene transcripts, and biofilm dynamics. Traditional methods such as inhibition zone assays, colony-forming units (CFUs), and basic microscopy, which were employed in previous studies [43,44], provide qualitative or semi-quantitative data. For instance, CFUs allow us to count only culturable bacteria, overlooking non-culturable populations, which can be crucial for understanding the complete microbial dynamics in biofilm communities. In contrast, RNA-based sequencing and RT-qPCR enable high-resolution analysis at the cellular level, capturing active metabolic processes and transcriptional activity [45]. This approach is particularly valuable in biofouling studies, where understanding the functional behavior of microbial communities is crucial for evaluating antibiofouling strategies. It allows for dynamic insights into population shifts, microbial metabolism, and transcriptional regulation, which cannot be captured through traditional assays. Further details on the protocols and analyses, including primer sequences, amplicon library preparation, and data analysis pipelines, are provided in the Supplementary Information (SI Section 1 and 2).

*16S rRNA gene amplicon library preparation*

The 16S rRNA genes amplicon libraries targeting the bacteria, archaea, and eukaryote 16S/18S rRNA gene variable regions 4–8 (abeV48-A) were prepared according to a custom protocol. The forward and reverse primers used included custom 24-nucleotide barcode sequences, followed by sequences targeting the bacteria/archaea/eukaryote 16S/18S rRNA gene variable regions 4–5 (abeV45-A): [515FB] GTGYCAGCMGCCGCGGTAA and [926R] CCGYCAATTYMTTTRAGTTT [46]. Purification of the resulting amplicon libraries was

carried out using the standard CleanNGS SPRI beads protocol (CleanNA, NL) with a bead-to-sample ratio of 3:5. The eluted DNA was suspended in 25 μL of nuclease-free water (Qiagen, Germany). Subsequently, sequencing libraries were prepared from the purified amplicon libraries using the SQK-LSK110 kit (Oxford Nanopore Technologies, UK), following the manufacturer's protocol. Further details on bioinformatic processing and microbial community analysis are provided in the Supporting Information (SI, section 1 and 2).

*Quantification of 16S rRNA gene transcripts via RT-qPCR*

Functional abundance of 16S rRNA genes was assessed using reverse transcriptase quantitative polymerase chain reaction (RT-qPCR). The abundance of 16S rRNA genes was quantified per ng of isolated DNA using reverse transcriptase quantitative PCR (RT-qPCR), employing a broad-range qPCR probe and primer set. A standard curve was generated using a linearized plasmid containing the qPCR amplicon, as described previously. RT-qPCR assays utilized 1 μL of cDNA sample templates, with specific forward and reverse primers amplifying the qPCR amplicon from *E. coli* MG1655. The 16S rRNA gene transcripts from both uncoated and coated samples were quantified using a SYBR Green-based qPCR assay conducted on the iCycler iQ5 RT-PCR detection system (Bio-Rad Laboratories, Hercules, CA). Further details on RT-qPCR assays can be found in the Supplementary Information (SI, section 3)

### 2.6. Statistical analysis

All experimental data were presented as mean values ± standard deviation (SD). Statistical analysis was performed using SPSS 11.5. One-way ANOVA and Student *t*-tests were conducted to assess statistical significance both between and within groups. Statistical significance levels were indicated as *$p < 0.05$, **$p < 0.01$, and ***$p < 0.001$.

## 3. Results and discussion

In Sections 3.1 to 3.3, we present the detailed surface modification, characterization, and antibiofouling assessments. Section 3.4 provides a comprehensive discussion, integrating these findings to elucidate the underlying mechanisms of the antibiofouling efficacy of our proposed surface coating.

### 3.1. Surface modification and characterization

The coating process was carried out through either *in-situ* synchronous assembly, involving the pumping of dopamine solutions through the membrane module, or an *ex-situ* dip-coating process under shaking conditions at room temperature. The successful deposition of the PDA-SP coating was confirmed by the distinct brown coloration observed on feed spacers and membranes, distinguishing them from their uncoated counterparts as shown in Fig. 2a, b and c. This coloration, attributed to catechol and amine groups in polydopamine, indicates successful polymerization and deposition of the coating onto the PP surface [47]. The PDA layer acts as a primer, enhancing the adhesion of hydrophilic layers like SP and cTA onto the hydrophobic PP substrate. This design not only ensures stable coating deposition but also supports subsequent functionalization processes, as evidenced by the uniform coloration observed on the coated surfaces (Fig. 2b). Notably, a cross-hatch pattern appeared on the membrane surface, indicating incomplete coating coverage in areas where the spacer made contact with the membrane during *in-situ* modification (Fig. 2b). Conversely, coupons coated under *ex-situ* conditions exhibited complete surface coverage of the coating, as depicted in Fig. 2c. While the observations distinctly illustrate the variability in coating uniformity between *in-situ* and *ex-situ* application methods (Fig. 2b, c, e, and f), the core focus of this research has been to evaluate the coating's effectiveness in reducing biofouling across a range of operational conditions. Future studies will explore how these application methods influence biofilm dynamics, aiming to enhance our understanding of their impacts in practical settings. This approach ensures that our findings are directly applicable to improving seawater reverse osmosis systems.

#### 3.1.1. Surface hydrophilicity

The static water contact angle (WCA), a measure of surface wettability, showed significant differences between coated and uncoated surfaces (Fig. 3a and b). The uncoated PP feed spacer exhibited a WCA of 135.5 ± 0.7°, indicative of its inherent hydrophobicity. In contrast, the

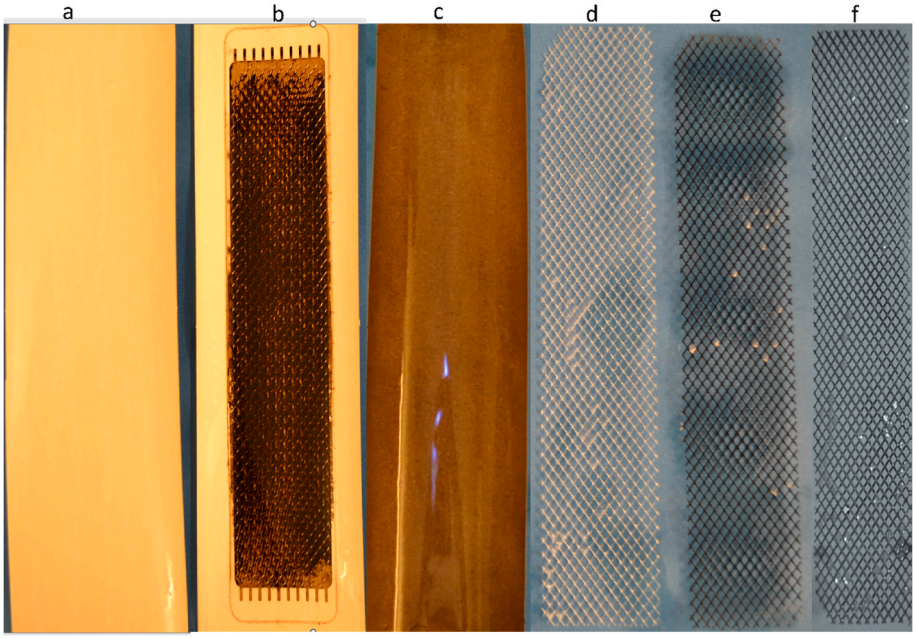


**Fig. 2.** Comparison of *in-situ* and *ex-situ* membrane and feed spacer modifications: (a) uncoated membrane, (b) *in-situ* PDA-SP-cTA coated membrane showing a crosshatch pattern from contact with the feed spacer, (c) *ex-situ* PDA-SP-cTA coated membrane without the pattern, indicating no contact during coating, (d) uncoated feed spacer, (e) *in-situ* PDA-SP-cTA coated feed spacer, and (f) *ex-situ* PDA-SP-cTA coated feed spacer. The brown color denotes the PDA-SP-cTA polymer coating. (For interpretation of the references to color in this figure legend, the reader is referred to the Web version of this article.)

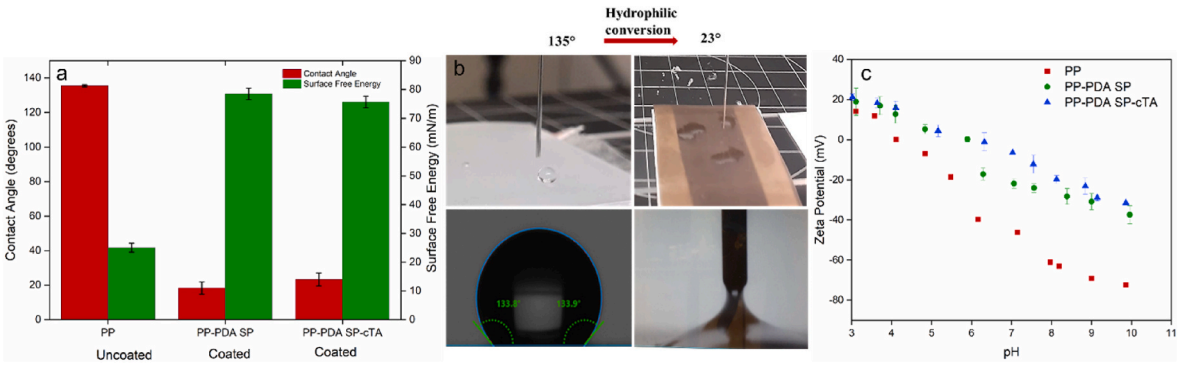


**Fig. 3.** Evaluation of surface properties: (a) Water Contact Angle (WCA) and Surface Free Energy (SFE) measured from static contact angle measurements. (b) Comparative representation of WCA and wettability between uncoated and PDA-SP-cTA coated PP surfaces. (c) Zeta potential profiling at acidic, neutral, and alkaline pH values for both uncoated and PDA-SP-cTA coated PP.

PP surface modified with PDA-SP and PDA-SP-cTA demonstrated remarkable hydrophilicity, with WCAs of 16 ± 4° and 23 ± 4°, respectively. This dramatic transformation is primarily attributed to the oxidative degradation by SP in the case of PP-PDA-SP, leading to an abundance of hydrophilic carboxylate groups [19]. Additionally, the interaction between the PDA-SP-coated surface and citric acid-blended tannic acid (PP-PDA-SP-cTA) further enhances hydrophilicity, involving chemical bonding of TA's hydroxyl and carboxylic acid groups with the amine groups in the PDA coating. These modifications significantly alter the surface chemistry of the PP feed spacers, transforming them from inherently hydrophobic to highly hydrophilic.

### 3.1.2. Surface free energy and wettability

We determined the surface free energy of the modified PP spacers using the Owens two-liquid method [32] based on measured WCA values. The surface energies of the polymer-coated spacers, PDA-SP (79 ± 2 mN/m) and PDA-SP-TAc (76 ± 2 mN/m), exceeded that of the uncoated PP (25 ± 2 mN/m) (Fig. 3a). The wetting behavior of water droplets on the coated surface differed significantly from that on the uncoated PP, as depicted in Fig. 3b. Water droplets readily spread and fully wetted the PP-PDA-SP coated surface upon contact, while failing to wet the hydrophobic uncoated surface. These findings highlighted the increased hydrophilicity, altered wetting behaviors, and enhanced surface free energy of the modified surfaces, consistent with similar surface functionalization studies conducted on different materials under various conditions [34].

### 3.1.3. Surface charge properties

The surface charge properties of both uncoated and coated PP materials were assessed via zeta potential measurements using streaming potential analysis over a pH range of 3.0–10.0 (Fig. 3c). The zeta potential of the uncoated PP surface was positive at pH 3.0–4.0 and shifted towards negativity as the pH increased from 4.0. This transition indicated a net negative surface charge of −65 mV, primarily due to the presence of polar molecules like hydroxyl and carboxylate groups [48]. In contrast, the PP-PDA-SP-coated surfaces exhibited a notable shift towards a less negative surface charge (−30 ± 4 mV), particularly at pH values above 5.5. This change resulted from the surface chemistry modifications induced by amine and phenolic hydroxyl groups present in the amphoteric PDA-SP. At low pH values, amine groups can undergo protonation from $–NH_2$ to $–NH_3^+$, introducing positively charged sites on the surface [49]. These charged sites generate an electric double layer on the PDA-SP coated surface, resulting in a shift toward a less negative potential for pH values above 6.0 compared to uncoated PP. Furthermore, subsequent surface modification with citric acid-blended tannic acid coating (PDA-SP-cTA) further increased surface charge at pH values above 6.5 (−12 ± 5 mV), attributed to carboxylic acid groups on the cTA surface. Additionally, the introduction of PDA-SP and cTA coatings shifted the isoelectric point of the coated surfaces to a more basic pH level compared to uncoated PP (pH 4.2). The observed shift in zeta potential upon coating suggests a more balanced surface charge distribution, which does not solely enhance fouling resistance through electrostatic repulsion. Instead, it implies the presence of a multifunctional surface where the interplay of hydrophilic modifications and other chemical functionalities collectively contribute to a less favorable environment for the adhesion of biofouling organisms, thereby reducing the propensity for biofouling.

### 3.1.4. Surface morphology

We evaluated the impact of polymer coatings on PP surface morphology using field emission scanning electron microscopy (FESEM) and analyzed the elemental composition through energy-dispersive X-ray spectroscopy (EDX). FESEM analysis was performed at various magnifications as required to reveal the surface and cross-sectional morphologies of both coated and uncoated PP spacers (Fig. 4a–f). Uncoated PP displayed a smooth surface (Fig. 4a), while PDA-SP and PDA-SP-cTA coatings exhibited surfaces covered with nanospheres, confirming successful deposition (Fig. 4b and c). At 40,000x magnification, the brown-colored PDA-SP-coated spacer exhibited a textured PDA nanoparticle coating film that adhered to the smooth surface of the PP (Fig. 4b). Additional cTA grafting onto the PDA-SP coating resulted in a more textured and rougher surface with irregular features, indicating successful TA deposition (Fig. 4c).

Elemental composition analysis via EDS mapping and spectral analysis revealed carbon (C), oxygen (O), nitrogen (N), and sodium (Na) as the primary elements in the PDA-SP coating layer (Fig. 4e). In contrast, uncoated PP predominantly comprised carbon atoms (Fig. 4d) [50]. The presence of nitrogen in the PDA-SP layer could be attributed to the amino groups within the PDA structure. The relative atomic content in PDA-SP-coated PP was found to consist of 79.7 % carbon, 6.4 % nitrogen, 13.1 % oxygen, and 1.53 % sodium (Table 2a). Similarly, the EDS spectral analysis of PDA-SP-cTA coated surface reveals the presence of carbon (C) and oxygen (O) (Fig. 4f). For the cTA-coated PP, the atomic content was determined to be 76.4 % carbon, 6.1 % nitrogen, and 17.3 % oxygen (Table 2a). The higher oxygen content is due to the presence of carbon, hydrogen, and oxygen atoms in the tannic acid polymer [51–53]. The cross-sectional analysis confirmed that the PDA-SP layer conforms closely to the PP surface, demonstrating a highly conformal coating with variable thickness across the entire cross-section (Fig. 4g–i). Similarly, cross-sectional SEM images of the PDA-SP-cTA coating showed a distinct coating layer across the surface, with varying thicknesses observed in different regions. The relative atomic content in PDA-SP-coated PP was 95.32 % carbon, 1.29 % nitrogen, and 3.28 % oxygen, respectively (Table 2b). Carbon, nitrogen and oxygen atomic content in PDA-SP-cTA coated PP was 88.96 % carbon, 0.92 % nitrogen, and 11.03 % oxygen, respectively (Table 2b). Overall, FESEM

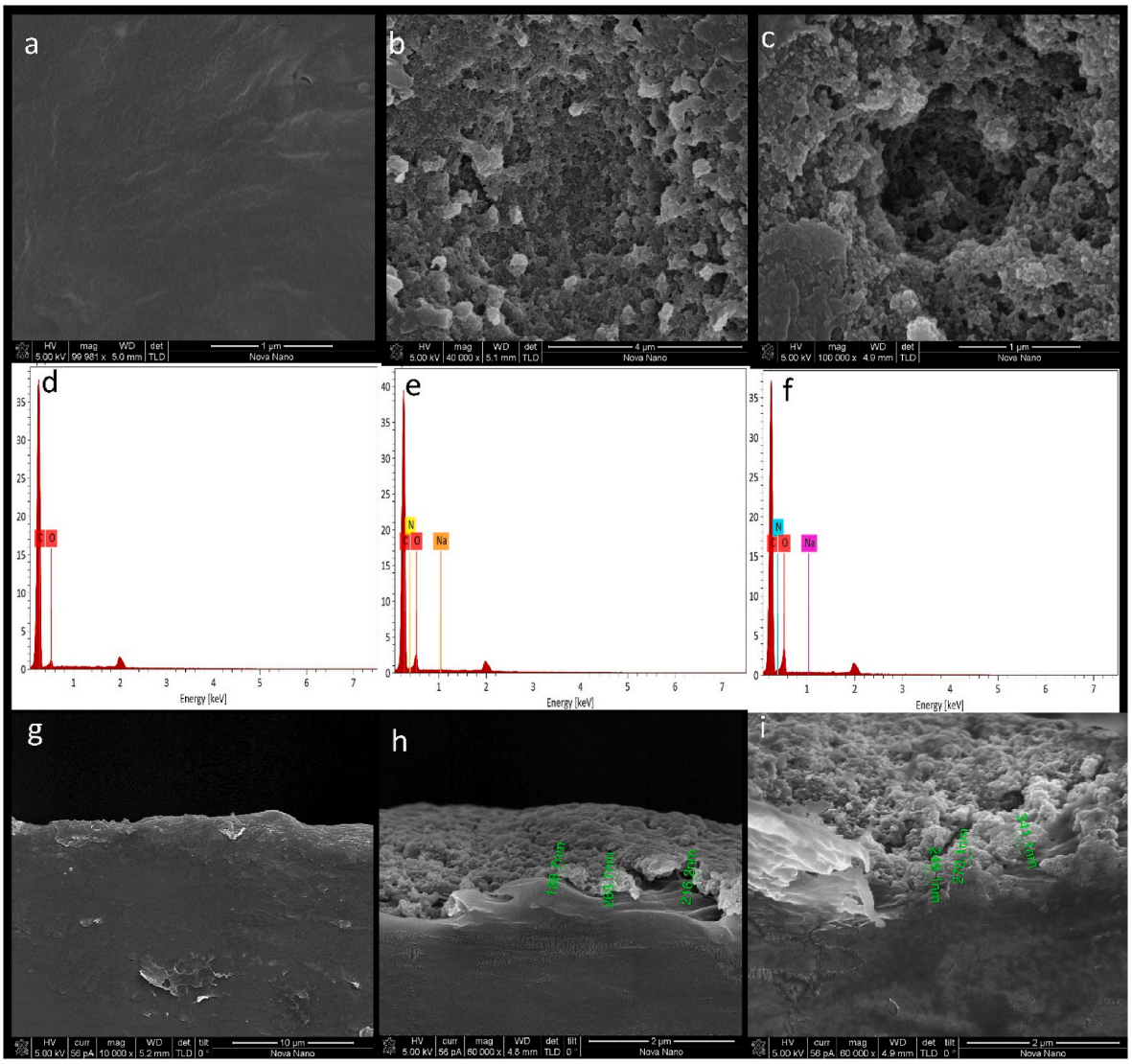


**Fig. 4.** Surface morphology and Elemental analysis: (a–c) Top panels present FESEM micrographs of (a) uncoated (b) PDA-SP, and (c) PDA-SP-cTA coated PP surfaces, alongside the bottom panels showing corresponding EDS spectra. (g–i) Surface cross-section; SEM cross-section images of (g) uncoated, and PDA SP and PDA-SP-cTA coated PP surfaces at a magnification of 50,000 × (scale bar: 10 μm).

**Table. 2a**
Relative surface atomic concentrations of uncoated and PDA-SP-cTA coated PP as determined by EDS spectra analysis.

| Samples | Atomic Percent (%) | | | | Atomic Ratio | |
|---|---|---|---|---|---|---|
| | C | N | O | Na | N/C | O/C |
| PP | 95.37 | – | 4.63 | – | – | 0.04 |
| PP- PDA-SP | 79.78 | 6.39 | 13.13 | 1.53 | 0.08 | 0.17 |
| PP- PDA-SP- cTA | 76.41 | 6.09 | 17.28 | 0.13 | 0.08 | 0.23 |

**Table. 2b**
EDS analysis of relative atomic concentrations in cross-sections of uncoated and PDA-SP-cTA coated PP.

| Samples | Atomic Percent (%) | | | Atomic Ratio | |
|---|---|---|---|---|---|
| | C | N | O | N/C | O/C |
| PP | 99.76 | – | 0.18 | – | 0.002 |
| PP- PDA-SP | 95.32 | 1.29 | 3.28 | 0.014 | 0.034 |
| PP- PDA-SP- cTA | 88.96 | 0.92 | 11.03 | 0.013 | 0.123 |

and EDS findings provided evidence of successful polymer coating incorporation onto the PP surface.

### 3.1.5. *Surface chemistry*

To investigate the possible presence of PDA-SP and cTA layers on the PP substrate, Attenuated Total Reflection Fourier Transform Infrared (ATR-FTIR) spectroscopy was employed. The FTIR spectrum indicated notable distinctions from the uncoated PP surface, suggestive of coating deposition as shown in Fig. 5.

*Hydroxyl and Carbonyl Group Analysis*: A broad absorption peak ranging from 3500 to 3200 $cm^{-1}$ highlighted the stretching vibrations of hydroxyl groups (-OH), indicative of the hydrophilic nature of the PDA-SP coating. This observation suggests an enhancement in surface wettability and water affinity, which is crucial for reducing biofouling potential. Additionally, the detection of a peak at approximately 1723 $cm^{-1}$, associated with carbonyl (C═O) functional groups, points to potential interactions facilitated by the oxidative actions of sodium periodate on PDA. These interactions may enhance the hydrophilicity of the surface, aligning with findings reported in the literature [19].

*Aromatic and Amine Group Analysis*: Peaks at 1613 and 1540 $cm^{-1}$ were identified, representing the superposition of phenylic C═C

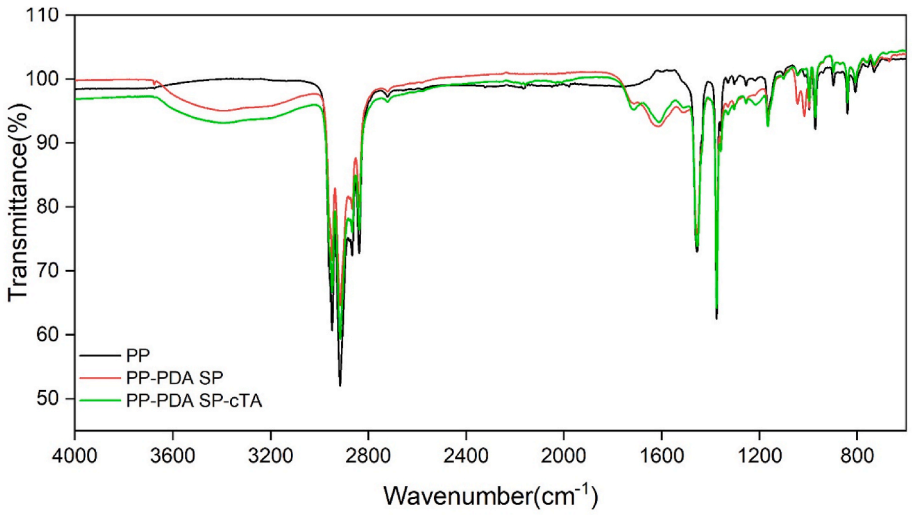


**Fig. 5.** Surface chemistry: FTIR spectra of uncoated and PDA-SP-cTA coated PP surfaces, highlighting distinct absorption peaks indicative of successful coating.

stretching and N–H vibrations. These peaks indicate the presence of aromatic ring structures and amine groups, which are typical in polydopamine coatings and critical for the subsequent layering of SP and cTA [46].

*Non-Covalent Interactions and Layer Formation*: The spectrum further revealed signals around 1050 and 1000 $cm^{-1}$, confirming the presence of oxygen-containing functional groups and C–C linkages, which likely contribute to the structural stability and mechanical integrity of the coating. Unlike traditional PDA coatings, where auto-oxidation by ambient oxygen does not yield bands associated with carbonyl and carboxyl groups, the sodium periodate oxidation at acidic pH (pH 5.0) appears to facilitate the formation of additional hydrophilic carboxyl groups on the substrates. This modification likely imparts extremely hydrophilic properties to the PP substrate, potentially enhancing the substrate's interaction with subsequent coating layers and improving overall biofouling resistance [19]. This phenomenon, documented in previous studies, underscores the innovative aspect of our coating process, which leverages chemical modifications to enhance functional performance [19].

*Additional spectra of PDA-SP-cTA Coating:* In the FTIR spectra of PDA-SP-cTA spacers, peaks at approximately 1715 $cm^{-1}$ might be associated with the stretching vibrations of carbonyl (C═O) functional groups [21]. Additionally, newly observed peaks at around 1620 $cm^{-1}$ (representing the C═O stretching vibration of carboxylic acid groups) and 1550 $cm^{-1}$ (reflecting the C═C stretching vibration of aromatic rings) could be attributed to the presence of phenolic compounds originating from both PDA and TA. Another prominent peak in the range of 3500 to 3300 $cm^{-1}$ was ascribed to the stretching vibration of –OH groups found in carboxylic acids and phenols [47], hinting at the hydrophilic contributions of tannic and citric acids. Although these peaks suggest the presence of PDA-SP and cTA on the PP surface, they do not conclusively confirm the deposition. To conclusively determine the composition and structural integrity of the PDA-SP-cTA coating, further detailed analysis is warranted. Advanced spectroscopic techniques such as X-ray photoelectron spectroscopy (XPS) and microscopic techniques including scanning electron microscopy (SEM) and transmission electron microscopy (TEM) are recommended. These methods will allow for a more precise characterization of the molecular interactions and confirm the presence of each component within the coating, addressing current knowledge gaps and enhancing the understanding of the coating's functional mechanisms.

*Proposed Layering Mechanisms and Theoretical Chemical Interactions*: The layering of citric acid and tannic acid onto the PDA-SP base is hypothesized to occur through hydrogen bonding and potential ionic interactions. These interactions are anticipated to be facilitated by the surface chemistry of the PDA layer, influenced by the application's pH and environmental conditions. The PDA layer is intended to act as a foundational primer, providing reactive catechol and amine groups that are hypothesized to support the stable deposition of SP and cTA. This may enhance the overall adhesion and structural stability of the coating. Citric acid is postulated to improve the hydrophilicity, structural integrity, and functional properties of the tannic acid layer through electrostatic and hydrogen bonding interactions, which are expected to contribute to the coating's stability and performance. Fig. S1 in the Supplementary Information illustrates these proposed interactions, depicting the non-covalent bonds and layer formation processes. The presence of functional groups, particularly hydroxyl and carbonyl groups, is suggested to enhance the coating's biofouling resistance and mechanical stability by potentially increasing hydrophilicity, which could decrease the surface's propensity for biofilm formation. Further studies are necessary to explore these interactions and assess the functional performance of the coating in-depth.

### 3.2. Antibiofouling assessments: long-term biofouling simulation experiments

#### 3.2.1. Impact of coating on feed channel pressure drop development

Feed channel pressure drop (FCP) was continuously monitored as an indicator of biofilm development, measured as a relative pressure drop (RPD) increase. For the positive control membrane fouling simulators (MFSs) with uncoated spacers that received nutrients, a threshold of a 300 % RPD increase was established to signify significant biofilm development, against which the performance of coated MFS units was compared. Over the five-day study period, negative control MFSs (labeled as UC-S, IC-S, and EC-S) containing coated and uncoated spacers without nutrient dosage did not show any significant RPD development (yellow and blue traces, Fig. 6a and c). As expected, the positive control MFSs (UC), which received nutrients with uncoated membranes and spacers displayed a continuous increase in RPD from the third day onwards (red trace, Fig. 6a and c). This substantial rise in FCP indicated accelerated biofilm development. By the end of the five-day experimental period, these monitors showed a notable 220 ± 30 % RPD increase (Fig. 6b and d). In contrast, MFS units containing both *in-situ* and *ex-situ* coated MFSs (IC) with nutrient dosing exhibited an RPD of 30 ± 20 % (Fig. 6b and d). This suggests that both *in-situ* and *ex-situ* modifications substantially reduce biofilm accumulation, enhancing long-term biofouling resistance compared to uncoated controls.

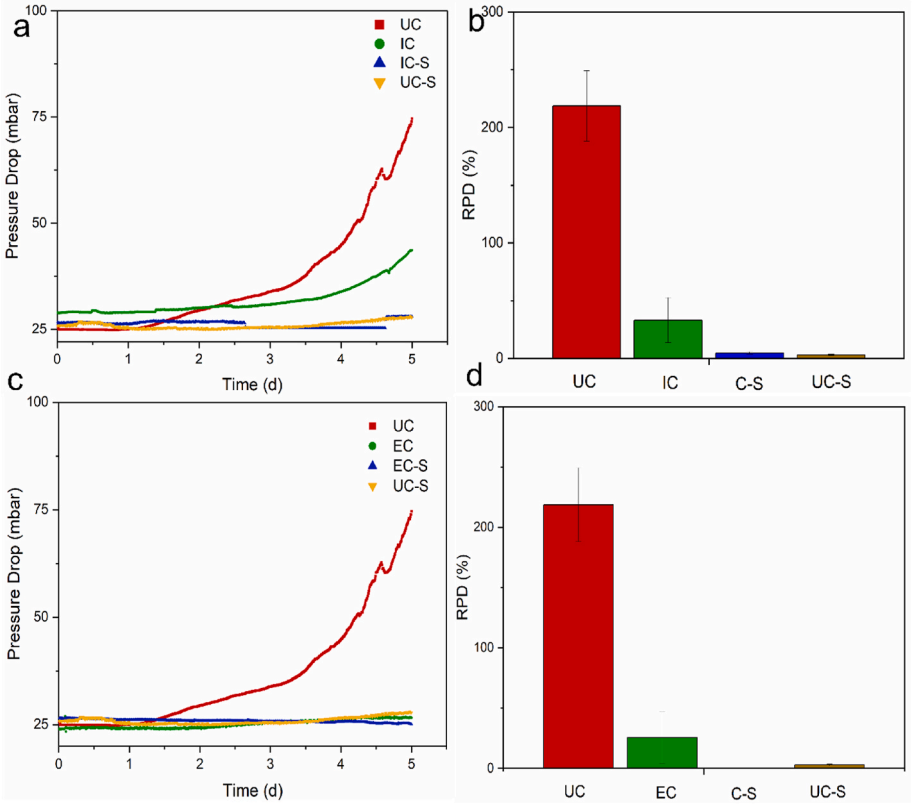


**Fig. 6.** MFS performance parameters over five days. (a) Feed channel pressure drop and (b) relative pressure drop (RPD) due to biomass accumulation in *in-situ* (top panel, a and b) and *ex-situ* coated MFS (bottom panel, c and d). Error bars represent data from independent triplicate MFS experiments. Abbreviations: UC; Uncoated with substrate, UC-S; Uncoated without substrate, IC; *In-situ* coated with substrate, IC-S; *In-situ* coated without substrate, EC; *Ex-situ* coated with substrate, EC-S; *Ex-situ* coated without substrate.

### 3.2.2. *Impact of coating on biofilm spatial distribution and structure*

The two-dimensional OCT images highlighted distinct differences in biofilm distribution and structures under the tested conditions at the end of the study (Fig. 7). The uncoated control MFS, when dosed with nutrients, exhibited mature biofilm coverage characterized by uneven distribution, varying thickness, and localized areas of high biofilm density (Fig. 7, labeled as UC) at the inlet, middle, and outlet positions of the MFS (Fig. S2). Additionally, uncoated feed spacers displayed a higher prevalence of biofilm streamers, which can pose challenges such as flow blockage, membrane fouling, and disruption of fluid dynamics in

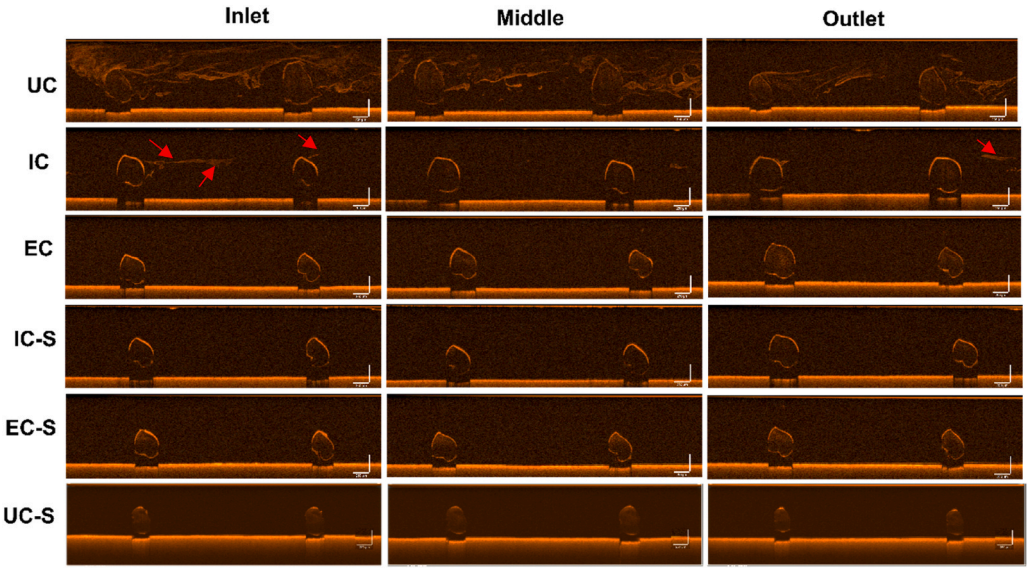


**Fig. 7.** Spatial biofilm distribution on uncoated (UC) and coated (IC and EC) membranes and spacer surfaces at the end of each experiment evaluated using 2D cross-sectional OCT scans at the inlet, middle, and outlet of each MFS. Red arrows indicate streamer formation observed in *in-situ* coated MFS. Abbreviations: UC, Uncoated with substrate; IC, *In-situ* coated with substrate; EC, *Ex-situ* coated with substrate; UC-S, Uncoated without substrate; IC-S, *In-situ* coated without substrate; EC-S, *Ex-situ* coated without substrate. (For interpretation of the references to color in this figure legend, the reader is referred to the Web version of this article.)

water filtration processes (Fig. 7, labeled as UC) [54,55]. Biofilm streamers are filamentous structures composed of bacterial cells embedded in a matrix of extracellular polymeric substances (EPS). These streamers are commonly associated with microbial communities that are more resistant to detachment, exhibit enhanced adhesion, and have a greater potential for biofouling [55]. Consequently, this leads to an increase in feed channel pressure drop as observed in the uncoated control MFS (Fig. 6a–Section 3.4). Furthermore, biofilm streamers serve as reservoirs of nutrients, thereby facilitating the colonization of other biofilm-forming bacteria and exacerbating biofouling [56]. In contrast, coated feed spacer surfaces displayed a thinner and more compact biofilm coverage with constrained growth patterns (Fig. 7, labeled as IC). Specifically, the *in-situ* coated feed spacer surface exhibited controlled biofilm growth with only a few strands of biofilm streamers at the inlet (Fig. 7, labeled as IC). However, no streamers or loose aggregates were found at the middle and outlet, indicating controlled and restricted biofilm growth patterns (Fig. 7, labeled as IC- middle and outlet). On the other hand, *ex-situ* coated feed spacers showed no biofilm streamers at any of the tested locations and had the thinnest biofilm coverage among the tested conditions (Fig. 7, labeled as EC). The absence of these structures suggests that the applied coating inhibited the attachment and colonization of filamentous bacteria or other microorganisms that tend to form biofilm streamers. Furthermore, the surfaces of the membranes treated with both *ex-situ*a nd *in-situ* coating methods did not exhibit any signs of biofilm formation, indicating the effectiveness of the applied coating in controlling biofouling. In the negative controls, which included both uncoated and coated MFS without nutrient dosage, no biofilm formation was detected on either the membrane or feed spacer surfaces (Fig. 7, labeled as UC-S, IC-S, EC-S).

Further quantitative analysis of biofilm thickness from OCT scans supported these findings (Table 3). The uncoated feed spacer (UC) exhibited significant variation in thickness across its surface with average values of $1 \pm 1$ mm at the inlet, $1.2 \pm 0.8$ mm in the middle, and $1.0 \pm 0.7$ mm at the outlet. In contrast, the *in-situ* coated surface (IC) displayed a more uniform biofilm thickness, averaging $0.71 \pm 0.05$ mm at the inlet, $0.8 \pm 0.7$ mm in the middle, and $0.6 \pm 0.9$ mm at the outlet. This represents an average thickness reduction of 36.9 %, 38.1 %, and 36.5 % at the inlet, middle, and outlet, respectively, compared to the uncoated control. The *ex-situ* coated surface displayed even greater biofouling resistance, as evidenced by the absence of biofilm streamers and the minimal biofilm thickness across all tested locations. By day 5, it showed the thinnest biofilm thicknesses, with $0.12 \pm 0.05$ mm at the inlet, $0.07 \pm 0.03$ mm in the middle, and $0.04 \pm 0.01$ mm at the outlet (Table 3). These measurements indicate thickness reductions of 89.4 %, 94.1 %, and 95.7 % at the inlet, middle, and outlet, respectively, in comparison to the uncoated control. These findings highlight the distinct advantages of the PDA-SP-cTA coating in effectively resisting biofouling through both *in-situ* and *ex-situ* methods. The coating not only inhibits biofilm growth but also promotes a more controlled and uniform biofilm formation, crucial for reducing issues like flow blockage, increased pressure drop, and reduced membrane permeability in membrane-based processes [54,56]. The *ex-situ* coating, in particular, demonstrates enhanced resistance to localized biofilm accumulation and detachment. By regulating biofilm distribution, reducing biomass accumulation, and inhibiting streamer formation, the coating significantly enhances the efficiency and longevity of biofouling-prone systems. It could also reduce and/or simplify biofilm removal and cleaning processes, making system maintenance and operation more manageable.

**Table 3**
Time-resolved quantification of biofilm thickness on uncoated and PDA-SP-cTA coated feed spacers with and without substrate. Abbreviations: UC, Uncoated with substrate; IC, *In-situ* coated with substrate; EC, *Ex-situ* coated with substrate; UC-S, Uncoated without substrate; IC-S, *In-situ* coated without substrate; EC-S, *Ex-situ* coated without substrate.

| MFS | DAY | Fouling thickness, mm | | |
|---|---|---|---|---|
| | | Inlet | Middle | Outlet |
| UC | 0 | 0 | 0 | 0 |
| | 3 | 0.09 ± 0.05 | 0.12 ± 0.04 | 1.00 ± 0.70 |
| | 5 | 1.00 ± 1.03 | 1.21 ± 0.81 | 1.00 ± 0.71 |
| IC | 0 | 0.02 ± 0.00 | 0.03 ± 0.00 | 0.01 ± 0.00 |
| | 3 | 0.04 ± 0.02 | 0.05 ± 0.03 | 0.05 ± 0.01 |
| | 5 | 0.71 ± 0.05 | 0.8 ± 0.70 | 0.6 ± 0.90 |
| IC-S | 0 | 0.02 ± 0.00 | 0.02 ± 0.00 | 0.02 ± 0.00 |
| | 3 | 0.02 ± 0.00 | 0.00 ± 0.00 | 0.01 ± 0.00 |
| | 5 | 0.02 ± 0.00 | 0.00 ± 0.00 | 0.00 ± 0.00 |
| EC | 0 | 0.02 ± 0.00 | 0.02 ± 0.00 | 0.01 ± 0.00 |
| | 3 | 0.02 ± 0.00 | 0.00 ± 0.00 | 0.02 ± 0.00 |
| | 5 | 0.12 ± 0.05 | 0.07 ± 0.03 | 0.04 ± 0.01 |
| EC-S | 0 | 0.03 ± 0.00 | 0.03 ± 0.00 | 0.02 ± 0.00 |
| | 3 | 0.03 ± 0.00 | 0.03 ± 0.0 | 0.02 ± 0.00 |
| | 5 | 0.03 ± 0.00 | 0.03 ± 0.00 | 0.02 ± 0.00 |

### 3.2.3. Impact of coatings on biomass accumulation: TCC, ATP, and TOC analysis

To quantitatively assess the antibiofouling performance of the surfaces, we conducted a comprehensive autopsy analysis on all MFSs after five days of operation. Flow cytometry (FCM) measurements were used to determine TCC values at the inlet, middle, and outlet positions, providing insights into the coating's impact on biofilm growth and colonization. The uncoated control MFS had notably higher TCC values of $2.8 \pm 0.2 \times 10^8$ cells/cm$^2$ at the inlet, $1.6 \pm 0.3 \times 10^8$ cells/cm$^2$ at the middle, and $1.39 \pm 0.03 \times 10^7$ cells/cm$^2$ at the outlet (Fig. 8a). These results indicated greater biofilm growth and colonization on the uncoated surfaces. In contrast, both the *in-situ* and *ex-situ* coated MFS units exhibited significantly lower TCC values. The *in-situ* coated MFS showed an approximate 85.5 % decrease in TCC at the inlet, 63.1 % decrease at the middle, and 84.8 % decrease at the outlet positions, respectively (Fig. 8a) compared to the uncoated control (*t*-test, $p > 0.05$), highlighting a significant decrease in biofilm formation. Furthermore, the *ex-situ* coated MFS units exhibited significantly greater reductions in TCC values compared to the uncoated control and *in-situ* coated MFS (Fig. 8a). At the inlet, the TCC decreased by approximately 90.1 %, while at the middle and outlet positions, TCC values were reduced by 93.3 % and 91.1 %, respectively. The lower TCC values on the coated MFS indicated a decreased presence of bacterial cells, highlighting the effectiveness of the PDA-SP-cTA coating in reducing bacterial attachment and colonization on both the membrane and feed spacer surfaces. These findings emphasize the antiadhesive and antibacterial properties of the applied coating.

We conducted ATP analysis to assess microbial activity and cellular viability on both coated and uncoated surfaces. ATP is a reliable indicator of microbial activity and metabolic state within biofilms [57]. Comparing the coated MFS samples to the uncoated control MFS, we observed a significant reduction in ATP concentrations, signifying decreased microbial activity and biofilm formation. The uncoated control MFS had an ATP concentration of $1.61 \pm 0.4 \times 10^4$ pg/cm$^2$ at the inlet position (Fig. 8b). In contrast, both the *in-situ* and *ex-situ* coated MFS displayed lower ATP concentrations at the inlet, measuring $0.41 \pm 0.02 \times 10^4$ pg/cm$^2$ and $0.42 \pm 0.01 \times 10^4$ pg/cm$^2$, respectively (Fig. 8b). This is a reduction of approximately 73.6 % and 73 %, respectively, compared to the uncoated control MFS. At the middle position, the uncoated control MFS had an ATP concentration of $0.6 \pm 0.2 \times 10^4$ pg/cm$^2$. In comparison, the *in-situ* coated MFS exhibited a reduced ATP concentration of $0.55 \pm 0.02 \times 10^4$ pg/cm$^2$ (11.8 % decrease), while the *ex-situ* coated MFS had an even lower concentration of $0.20 \pm 0.02 \times 10^4$ pg/cm$^2$, representing a reduction of approximately 67.6 %. At the outlet position, the uncoated control MFS had an ATP concentration of $0.6 \pm 0.10 \times 10^4$ pg/cm$^2$. The *in-situ* and *ex-situ* coated MFS displayed concentrations of $0.44 \pm 0.01 \times 10^4$ pg/cm$^2$ and $0.32 \pm 0.03 \times 10^4$ pg/cm$^2$, respectively. This corresponds to reductions of approximately 29.4 % and 48.1 % for the *in-situ* and *ex-situ* coated MFS

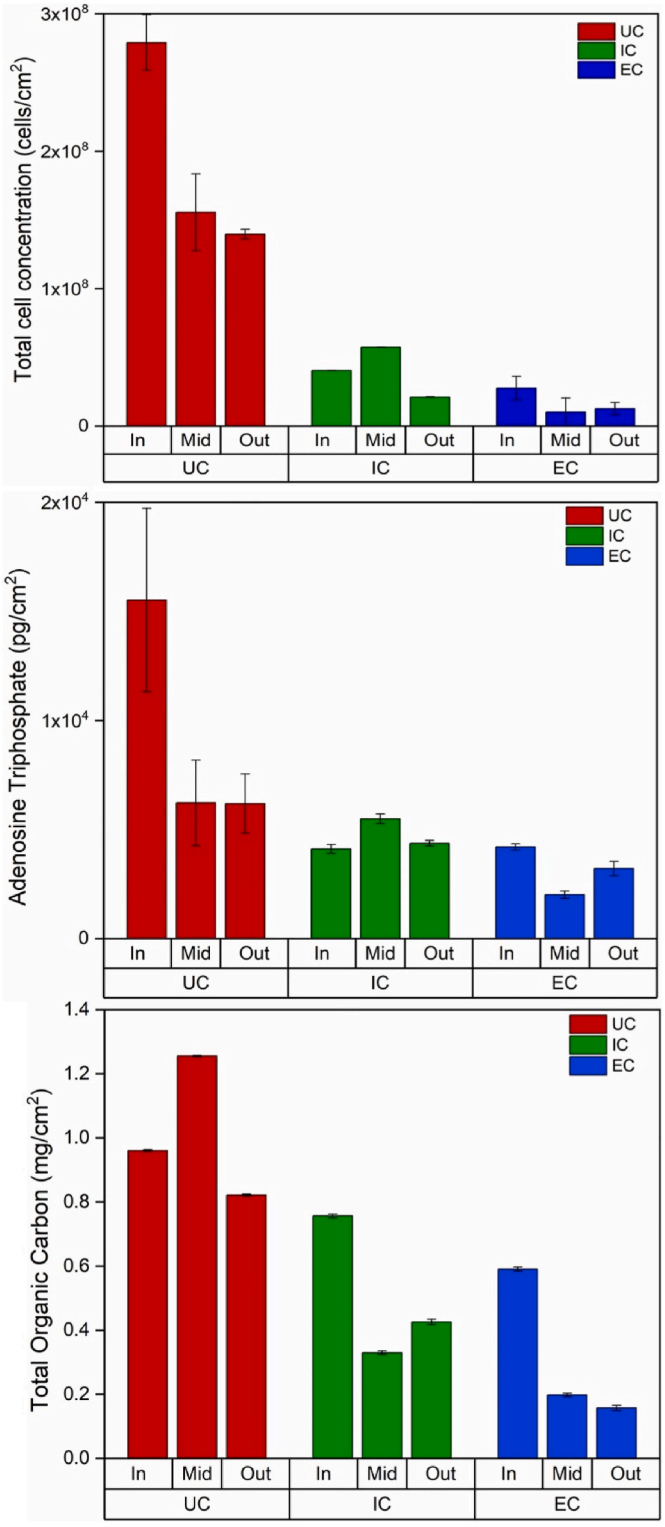


**Fig. 8.** Biomass quantification in MFSs: Comparative analysis of biomass metrics (a) TCC, (b) ATP, and (c) TOC for uncoated (UC) and coated (IC, EC) MFSs with substrate dosing.

compared to the uncoated control MFS. The observed reduction in ATP levels in coated MFS, particularly when normalized against total cell count, suggests a potential biocidal effect. The statistical analysis supports this, showing significant differences in normalized ATP levels (ANOVA, p-value = 0.017, F-statistic = 8.7), with post hoc tests confirming significant reductions in coated samples compared to uncoated (UC vs EC, p = 0.01; UC vs IC, p = 0.06). These reductions may result from impaired microbial cell membrane integrity, potentially causing leakage of intracellular components and disrupting processes including the electron transport chain, thus diminishing ATP production and energy metabolism [58]. Such alterations could also impact ATP synthesis-related enzymes like ATP synthase. While these findings suggest a biocidal action by the PDA-SP-cTA coating, particularly on a per-cell basis, they could also indicate reduced bacterial adhesion and proliferation. This necessitates further research for a definitive understanding of the coating's biocidal mechanism. In the negative controls, which included both uncoated and coated MFS without nutrient dosage, there was no significant biomass accumulation observed (Fig. S3, labeled as UC-S, IC-S, EC-S).

The TOC analysis revealed a marked decrease in organic carbon content on coated MFS compared to uncoated MFS (Fig. 8c). The higher TOC values (0.96 ± 0.003 mg/cm$^2$ at the inlet, 1.25 ± 0.002 mg/cm$^2$ at the middle, 0.82 ± 0.003 mg/cm$^2$ at the outlet) observed on the uncoated MFS indicated a greater accumulation of organic compounds on the membrane and feed spacer surface, providing a nutrient source for biofilm growth. This is likely attributed to the hydrophobic nature of the feed spacer, which offers a larger surface area and facilitates the adherence of organic compounds, including EPS produced by biofilms [24]. In contrast, both *in-situ* and *ex-situ* coated MFS showed substantial TOC reductions. The *in-situ* coated MFS exhibited a 21.2 % decrease at the inlet, 73.8 % in the middle, and 48.2 % at the outlet. The *ex-situ* coated MFS demonstrated even greater reductions, with approximately 38.5 % at the inlet, 84.7 % in the middle, and 80.8 % at the outlet compared to uncoated MFS (Fig. 8c). These findings suggest that the applied coating plays a crucial role in reducing TOC by preventing the adsorption and retention of organic compounds, thereby reducing their accumulation on the surface. Additionally, the high surface free energy of the coated surface promotes better wetting, facilitating the dispersion and removal of organic compounds during filtration [59]. This mechanism collectively contributes to the reduction of organic compound deposition and biofilm formation, ultimately leading to decreased TOC levels. The PDA-SP-cTA coating harnesses a synergistic biocidal effect, where each component plays a complementary role in preventing biofilm formation. The hydrophilic nature of PDA effectively reduces microbial attachment by creating a surface less favorable for microbial colonization [19,20], while sodium periodate induces oxidative stress, damaging microbial cells [25]. The phenolic and hydroxylic functional groups present in citric acid-blended tannic acid (cTA) interact with bacterial cell walls, and proteins, causing both chemical and physical damage to the microorganisms [22,23,26]. The observed reductions in ATP levels, and accumulated biomass, combined with the documented biocidal properties of PDA, SP, and TA in previous studies [19,24,59], support the potent biocidal effect of the PDA-SP-cTA coating on the membrane and feed spacer surface.

### 3.2.4. *Impact of coatings on EPS composition and distribution*

To further characterize the biofilm development, we investigated the influence of the PDA-SP-cTA coating on extracellular polymeric substances (EPS) production. EPS plays a crucial role in biofilm formation and stability, serving as a substrate for bacterial cell attachment and offering protection [60]. It also contributes to the structural support and acts as a source of nutrition for the microbial community within the biofilm. EPS comprises various components, including proteins and polysaccharides (carbohydrates), among others [61]. Of these, proteins and polysaccharides are the primary constituents and key indicators of EPS quantity. Notably, proteins are prone to denaturation and can form strong hydrophobic-hydrophobic bonds with hydrophobic substrates. Polysaccharides are typically hydrophilic, suggesting that they may be foulants on hydrophilic membranes [62]. Thus, understanding EPS composition and quantity provides insights into biofouling potential and antibiofouling coating effectiveness.

*3.2.4.1. Composition.* To assess changes in EPS, we quantified EPS in uncoated, *in-situ* coated, and *ex-situ* coated samples (Fig. 9a and b). *Ex-situ* coating exhibited a significant reduction of 91 ± 2 % in carbohydrates and 68.7 ± 0.1 % in proteins compared to uncoated samples. In contrast, *in-situ* coated samples showed a slight increase in protein levels by 4 ± 2 % and a 23 ± 0.7 % reduction in carbohydrates. These findings indicate that both *in-situ* and *ex-situ* coatings impact EPS production, with *ex-situ* coatings having a more pronounced effect. Furthermore, the protein to polysaccharide ratio of EPS on the PDA-SP-cTA modified samples was lower in coated samples compared to uncoated controls.

*3.2.4.2. EPS fraction profiling.* To further analyze variations in EPS fractions, we conducted a 3D fluorescence excitation-emission matrix (FEEM) analysis on biofilms developed on both PDA-SP-cTA coated and uncoated samples. This approach, using 3D-FEEM fluorescence spectroscopy, enabled indirect quantitative analysis of EPS through peak intensity measurements, allowing for the identification of specific fluorescence peaks linked to different EPS components. In the uncoated controls, four distinct peaks were evident (Fig. 9c): Peak I (approximately 230/295 nm) for tryptophan-microbial protein-like compounds, Peak II (around 230/240 nm) for tyrosine amino acid compounds, Peak III (around 340/345 nm) for fulvic acid-like substances, and Peak IV (380/345 nm) for humic acid-like substances, suggesting a pronounced presence of proteins and polysaccharides. This finding is consistent with the EPS quantification data presented in Fig. 9a and b. In contrast, *in-situ* coated samples displayed three peaks (Fig. 9d), and in *ex-situ* coated samples only two (Fig. 9e), signaling notable alterations in EPS composition due to the coating.

Our quantitative analysis revealed marked reductions in microbial protein-like substances and other EPS components in coated samples compared to uncoated controls. Specifically, *in-situ* coated samples exhibited reductions of 80 ± 4 % in microbial protein-like substances, 56.5 ± 0.03 % in tyrosine-like compounds, 10 ± 10 % in humic acid-like substances, and 87 ± 8 % in fulvic acid-like substances, compared to uncoated controls (Fig. 9f). In *ex-situ* coated samples, we observed a complete absence of tyrosine-like and fulvic acid-like substances, alongside an 89 ± 1 % reduction in protein-like compounds and a 40 ± 8 % decrease in humic acid-like substances (Fig. 9f). These findings indicate the PDA-SP-cTA coating's notable influence on the synthesis of microbial by-products and tyrosine substances, which may contribute to reduced biofouling. The reduction in EPS components, particularly in tyrosine-like and fulvic acid-like substances, highlights the coating's capacity to alter the biofilm matrix, potentially reducing biofilm adhesion and stability. EPS serves as a critical scaffold for microbial

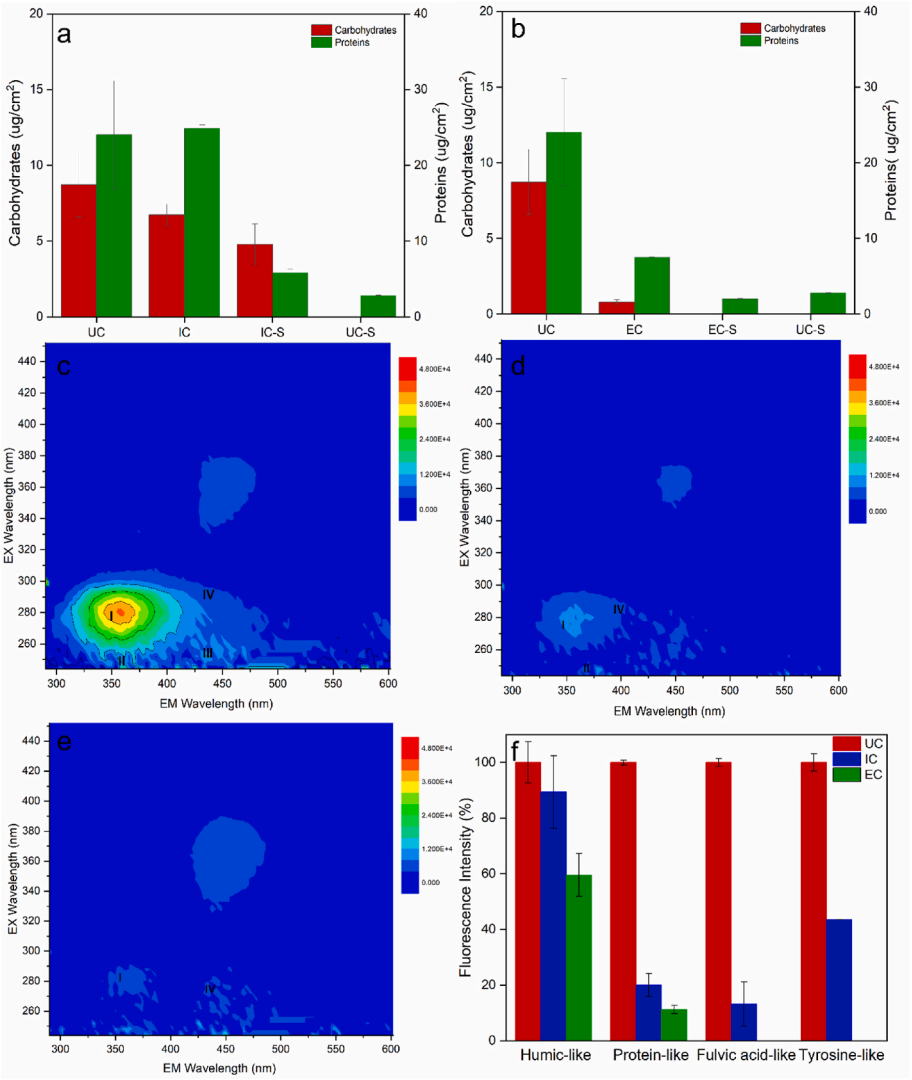


**Fig. 9.** EPS Composition and Spatial Distribution: (a, b) Protein and carbohydrate EPS content in *in-situ* and *ex-situ* coated samples. (c–e) 3D-FEEM EPS fraction profiles from uncoated, *in-situ*, and *ex-situ* coated MFS, indicating humic-like, protein-like, fulvic acid-like, and tyrosine-like substances. (f) Comparative fluorescence intensities for these substances post-biofouling.

attachment and structural support in biofilms, and its disruption can significantly impair biofilm formation. These changes align with observations of reduced biofilm cohesiveness in coated samples, where the simplified EPS composition further underscores the coating's impact on biofilm integrity.The observed reductions in EPS peak intensities in PDA-SP-cTA coated samples may indicate a multifaceted impact on biofilm biochemistry, possibly due to reduced bacterial counts or biofilm diversity changes. Normalization against bacterial counts revealed significant differences in EPS components (p-values: Humic-like = 0.0226, Protein-like = 0.0055, Fulvic acid-like = 0.0016, Tyrosine-like = 0.0033). Particularly, the absence of tyrosine-like and fulvic acid peaks in the *ex-situ* coated samples could reflect a more complex interaction between the coating and the biofilm matrix, possibly affecting both the biofilm's structural integrity and its metabolic activity. The pronounced reduction in EPS components, including proteins and polysaccharides, suggests that the PDA-SP-cTA coating inhibits microbial processes critical to EPS synthesis, further weakening biofilm stability. Given the significant differences in bacterial counts and EPS intensities, further studies are warranted to investigate the interplay between bacterial adhesion, EPS production, and diversity within the biofilm communities. The subsequent section will delve deeper into the molecular and functional profiles of microbial communities in biofilms on coated surfaces, offering a more detailed exploration of these complex interactions.

### 3.2.5. Impact of coating on microbial community diversity and activity

To assess total and active microbial communities in biofilms on both coated and uncoated samples, we employed DNA and RNA-based 16S rRNA amplicon sequencing techniques. Sequencing of the V4–V5 region using the ONT approach yielded 736,770 raw sequences, subsequently filtered to obtain 648,879 high-quality read pairs. The final dataset consisted of 648,879 read pairs, providing coverage ranging from 299,049 for uncoated samples to 349,830 for both *in-situ* and *ex-situ* coated samples. Non-chimeric, quality-filtered reads were clustered into 3,490 operational taxonomic units (OTUs) at a 97 % sequence similarity threshold. The number of OTUs detected varied among the samples, with uncoated control samples showing the highest diversity (Table S1).

*3.2.5.1. Biofilm diversity and structure.* To assess biofilm diversity and structure, we analyzed the species richness and diversity of DNA and RNA-based microbial communities in both uncoated and coated samples. Alpha diversity indices (Richness, Shannon-Wiener, and Simpson evenness) were calculated at a depth of 15,000 OTUs per sample (Table S1). The Shannon and Simpson diversity indices showed that uncoated control samples had higher bacterial diversity (Shannon: 4.28 and Simpson: 2.90) compared to coated samples (Shannon: 2.65 and Simpson: 1.60 for *in-situ*; Shannon: 2.01 and Simpson: 1.18 for *ex-situ*). RNA-based diversity analysis yielded similar results (Table S1), demonstrating decreased microbial diversity in coated samples relative to uncoated samples. Non-parametric t-tests confirmed significant differences in species richness and diversity indices between coated and uncoated samples, with no significant differences between *in-situ* and *ex-situ* coated subgroups. These results suggest that surface modification with PDA-SP-cTA led to lower diversity and evenness.

To visualize the differences in microbial community composition, we conducted a principal coordinates analysis (PCoA). PCoA visually represents dissimilarities in community composition by measuring distances between samples [63]. In our analysis, the PCoA plot captured 86.9 % of the variation in relative abundance across the dataset, with dissimilarities between uncoated samples and both *in-situ* and *ex-situ* coated samples (13.1 %) (Fig. S4a). RNA-based diversity analysis yielded a similar shift in the community structure (Fig. S4b). These findings indicated changes in the community structure of surface-coated samples, forming a distinct cluster separate from the uncoated control samples. In summary, surface modification with PDA-SP-cTA reduced microbial diversity and created a distinct community structure, potentially inhibiting biofouling microorganisms.

*3.2.5.2. Microbial community profiling.* We analyzed the microbial community composition in both uncoated and coated samples using DNA-based community profiling. This revealed substantial differences in the dominant genera and their relative abundances. The community composition was calculated based on percentages of the total OTUs, and a heatmap was generated at the genus level, identifying the 25 most abundant phylotypes in both libraries (Fig. 10a). Bacteria were found to dominate the total microbial communities in both the coated and uncoated samples.

In the uncoated samples, the DNA-based analysis indicated the prevalence of four dominant colonizers: *Alteromonas* (49.5 %), *Neptuniibacter* (35.2 %), *Myxococcota* (2.7 %), and *Salinimonas* (2.5 %). These genera are well known for their association with biofouling events and biofilm formation in marine environments [64,65]. Notably, *Alteromonas* species are recognized for their biofilm-forming capabilities and the production of extracellular polymeric substances (EPS), which contribute to biofilm stability and adhesion. *Alteromonas* is often linked to surfaces and particulate fractions in seawater and serves as a primary surface colonizer in coastal marine environments [66,67]. The dominance of *Alteromonas* in uncoated samples suggests that the hydrophobic surface of the uncoated feed spacer favored its adhesion and growth.

In contrast, the coated samples exhibited a reduced presence of *Alteromonas*, with only 6.5 % in *ex-situ* coated samples and 0.6 % in *in-situ* coated samples. The *in-situ* coated samples were largely dominated by *Neptuniibacter* (85 %), followed by *Bdellovibriota* (2.9 %), *Alternomonas* (1.7 %), *Myxococcota* (1.6 %), and a few other genera. Similarly, the *ex-situ* coated samples were mainly dominated by *Neptuniibacter* (81 %) with a lower abundance of *Alternomonas* (6.5 %). This reduction in *Alteromonas* abundance can be attributed to the hydrophilic properties induced by the PDA-SP-cTA coating, characterized by a lower water contact angle, higher surface free energy, and a net negative surface charge. Hydrophilic surfaces typically hinder the attachment and growth of hydrophobic bacteria like *Alteromonas* through electrostatic repulsion, following the DLVO theory's emphasis on electrostatic forces in bacterial adhesion [68,69]. This resulted in a less favorable environment for *Alteromonas* colonization and decreased abundance. Interestingly, the genus *Neptuniibacter* showed an increased abundance on the coated surfaces, accounting for 81 % in *ex-situ* coated samples and 85 % in *in-situ* coated samples, compared to 35 % in uncoated samples. *Neptuniibacter* is another halophilic, biofilm-forming genus frequently detected in coastal areas, including seawater, sediments, estuaries, and marine ecosystems [70]. It is important to note that *Neptuniibacter* is a relatively newly described genus, and ongoing research continues to expand our understanding of its diversity, ecological roles, and functional properties. The RNA-based findings corroborated these DNA trends, with *ex-situ* coated samples showing a pronounced rise in the relative abundance of *Neptuniibacter* and a decline in *Alteromonas*. Further RNA-based analysis details are available in the Supplementary Information (SI section 4 and Fig. S5).

In conclusion, the observed shift in microbial community composition on coated surfaces can be attributed to several factors. First, the coating compounds might have specific antimicrobial properties that are particularly effective against biofilm-forming genera *Alteromonas*, *Salinimonas*, *Myxococcota*, and *Oliebacter*, creating a selective advantage for *Neptuniibacter*. Second, the surface properties of the coating may have favored the initial attachment and colonization of the *Neptuniibacter* over other genera, leading to its preferential growth. Third, the coating might have altered the physical and chemical microenvironment, favoring the growth of *Neptuniibacter* and creating conditions unfavorable for the growth of other genera. The observed dominance of *Neptuniibacter* in the coated samples suggests a shift in biofilm dynamics compared to the uncoated controls dominated by *Alteromonas*,

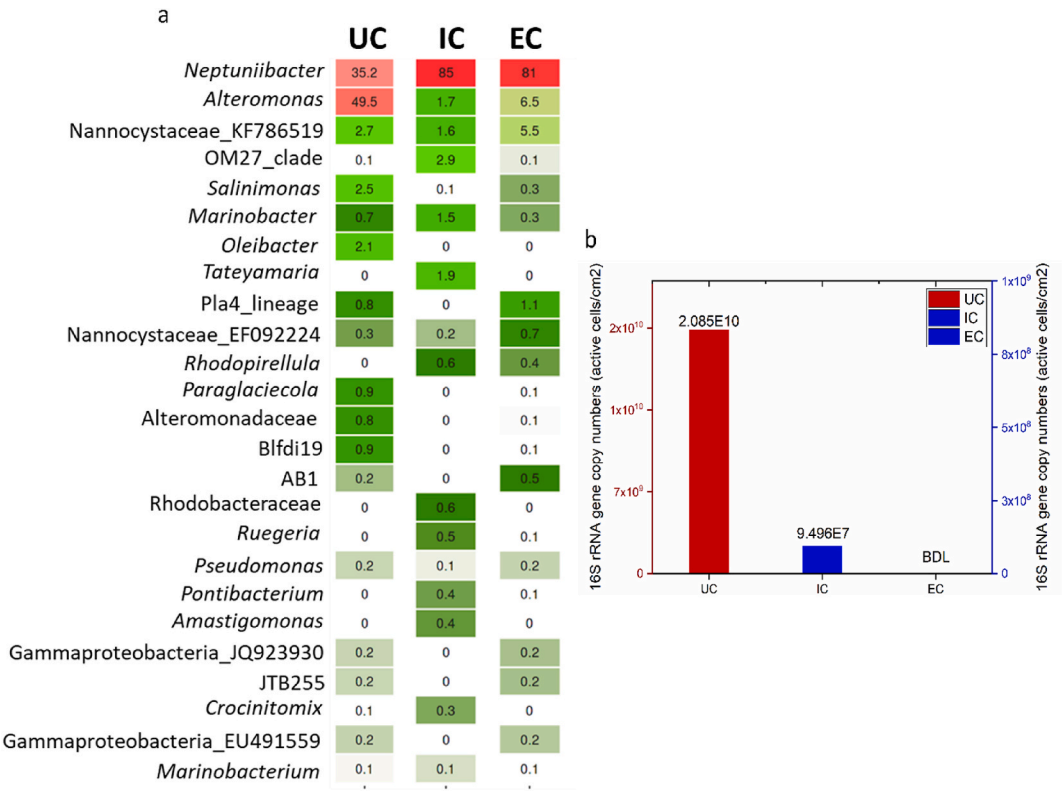


**Fig. 10.** Microbial community profiling in MFS Biofilms: Heatmap of the 25 most abundant microbial types identified in the biofilm samples of each MFS containing uncoated and coated membranes and spacers. (a) DNA-based total microbial communities. (b) RT-qPCR quantification of active bacterial gene copies. Abbreviations: UC - Uncoated, IC – *In-situ* coated, EC - *Ex-situ* coated.

potentially enhancing the long-term antibiofouling performance of the coatings. Further experimental studies, particularly pure culture investigations, are essential to confirm these effects and to understand the specific role of *Neptuniibacter* within biofilm matrices. Such studies could elucidate how *Neptuniibacter* impacts biofouling management and contribute to a deeper understanding of microbial population dynamics and biofilm stability on coated surfaces. Additionally, the noticeable reduction in *Alteromonas* underscores the population selection effect, highlighting the coating's efficacy in controlling biofouling and its potential to enhance the performance and sustainability of seawater desalination systems.

*3.2.5.3. Impact of coating on active microbial colonization: quantification assessed by RT-qPCR analysis.* To quantify active bacterial colonization, we extracted RNA and employed reverse transcription-quantitative polymerase chain reaction (RT-qPCR) targeting 16S rRNA gene transcripts. This analysis sheds light on the coating's effect on microbial colonization and activity, improving our understanding of its inhibitory mechanisms and biofouling mitigation potential. The results showed a significant reduction, with a 99.5 % decrease in 16S rRNA gene transcript copy numbers in *in-situ* coated samples compared to the uncoated controls. *Ex-situ* coated samples exhibited an even more pronounced effect, completely inhibiting active bacterial colonization with 16S rRNA transcripts falling below detectable levels (Fig. 10b). In summary, our microbial community studies revealed that surface coating significantly impacted microbial diversity, composition, and abundance within biofilms. The coating effectively reduced microbial diversity and altered the relative abundance of dominant genera, resulting in a distinct shift in the microbial community structure. Furthermore, the quantification of actively metabolizing cells provided concrete evidence of the coating's effectiveness in inhibiting bacterial colonization. These findings highlight the promising potential of the applied coating to mitigate biofouling and enhance seawater desalination system performance.

*3.2.5.4. Comparative efficacy of in-situ and ex-situ coating techniques.* Our comparative analysis of *in-situ* and *ex-situ* coating techniques reveals significant differences in their uniformity and antibiofouling performance. The *in-situ* method, which involves the direct application of coating solutions during operation, often results in uneven coverage. This is evident from the cross-hatch patterns observed on the membrane surfaces where spacers contact membranes or in zones of higher fluid dynamics, indicating incomplete coating. Such incomplete coverage can compromise the coating's effectiveness in operational settings. In contrast, the *ex-situ* application, involving a controlled dip-coating process, ensures comprehensive and uniform coating coverage. This method significantly enhances surface properties such as hydrophilicity and surface free energy, which are critical in resisting biofouling. Our results demonstrate that *ex-situ* coatings provide superior biofouling resistance. Long-term biofouling simulation experiments highlighted that *ex-situ* coatings effectively reduce biofilm thickness and restrict biofilm growth more significantly than in-situ methods. Additionally, quantitative assessments reveal that *ex-situ* coatings substantially decrease both total cell count (TCC) and active microbial colonization. The near absence of 16S rRNA gene transcripts in *ex-situ* coated samples underscores the profound impact of complete and even coating on inhibiting bacterial colonization. These findings highlight the pivotal role of thorough and uniform application in enhancing the coating's overall performance, making *ex-situ* coatings more effective for long-term biofouling control in seawater desalination systems.

### *3.3. Coating stability and durability assessment*

#### *3.3.1. Visual observations*

Visual inspections demonstrated the enduring stability of the characteristic brown color of the coating over time. This color remained

consistent across pH values of 1, 3, 7, and 10 throughout the entire 30-day study. However, at pH 13, a significant transformation became evident as reported earlier [52]. The initial brown color of the PDA-SP-cTA-coated PP surfaces gradually faded, turning pale white after just one day of exposure to the extremely alkaline environment (Fig. 11a). Further observations indicated substantial degradation beyond day 3 at pH 13, leading to the complete removal of the PDA-SP-cTA coating, leaving the PP substrate visibly clear and uncoated (Fig. 11a). The observed degradation at pH 13 aligns with known limitations of PDA-SP-based coatings in extreme alkaline environments [19], which are beyond the standard operating and cleaning conditions (pH 2.5–11) typically encountered in seawater reverse osmosis systems. These findings confirm the PDA-SP-cTA coating's robust performance within operational pH ranges, maintaining structural and functional integrity under these conditions.

### 3.3.2. IR spectroscopy

To complement visual findings, FTIR spectroscopy results provided critical insights into the chemical stability and durability of the coatings. Pristine PDA-SP-cTA-coated samples displayed three distinct characteristic peaks at 3330, 1720, and 1800 $cm^{-1}$, corresponding to hydroxyl and carbonyl groups (Fig. 11b–e). However, at pH 13, evident degradation occurred, marked by the near-complete disappearance of C═O ester bonds, and reduced intensity at 3300 $cm^{-1}$ on day 1 (Fig. 11b). This signified a substantial degradation of the coating in highly basic environments, a phenomenon exacerbated by rinsing for 24 h. Subsequently, at pH 13, the remaining PDA-SP-cTA coating on the PP substrate was completely removed, starting from day 3 (Fig. 11c, d,e). This was evident from both visual observations and FTIR spectra, which showed the complete disappearance of peaks at 3300, 1750, and 1650 $cm^{-1}$ (Fig. 11c, d,e). These findings align with previous research demonstrating that PDA coatings can dissolve in strong alkaline solutions, resulting in a color transition of the substrate to white [46]. Despite these observations, at pH values of 10 and 7, only minor differences in surface chemical composition were noted, showing initial signs of degradation but maintaining the coating integrity over the 30 days (Figs. S6f–j). These variations, reflected in reduced peak intensity and the partial disappearance of the 1730 $cm^{-1}$ peak, indicate some stability in this pH range. For pH values 1 and 3, the coatings demonstrated remarkable stability, with no significant alteration in the characteristic peaks, underscoring the coatings' resilience under acidic conditions (Fig. S6a). This enduring stability, particularly under the pH

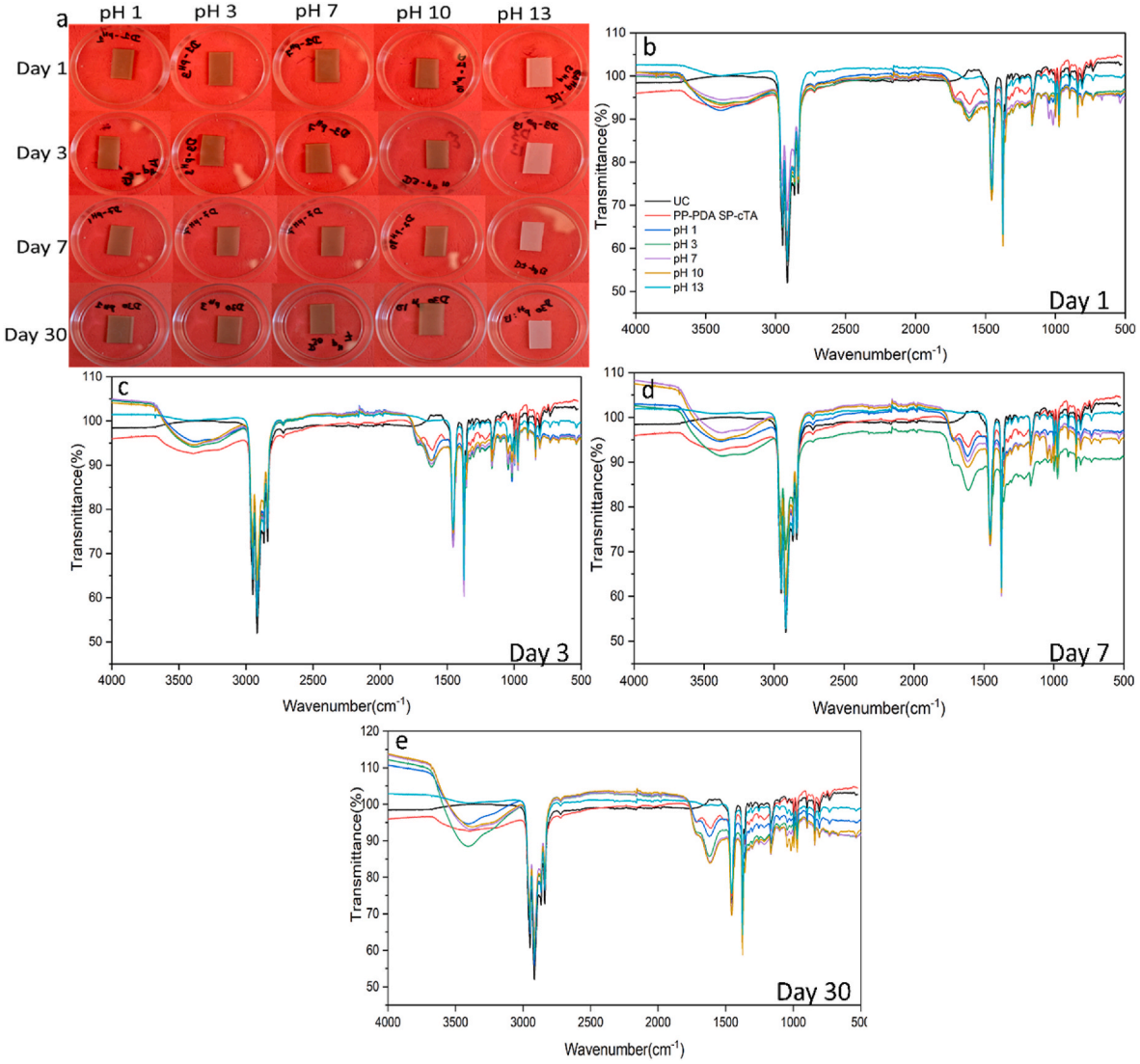


**Fig. 11.** Stability and durability assessment of the PDA SP-cTA coating under tested conditions: (a) Photograph showing color changes in the PDA SP-cTA coated PP surface shaken in aqueous solutions over time. (b–e) IR spectroscopy analysis of PDA SP-cTA coated spacers on days 1, 3, 7, and 30. (For interpretation of the references to color in this figure legend, the reader is referred to the Web version of this article.)

conditions typically encountered in seawater desalination systems, underscores the coatings' ability to maintain their integrity without releasing antimicrobial materials into the environment, emphasizing their minimal environmental impact. This highlights the crucial role played by sodium metaperiodate as an oxidant and citric acid as an additive in preserving the coating's integrity in acidic environments, as indicated in previous studies [19,26]. In conclusion, the PDA-SP-cTA coatings exhibited outstanding durability and stability, especially within pH conditions commonly encountered in practical membrane-based applications. Their ability to maintain structural integrity, external appearance, and chemical composition over extended periods, particularly in acidic and neutral settings, positions them as a dependable choice for combating biofouling in diverse industrial settings. Consequently, future research may focus on refining the coating formulation to enhance its stability across a broader pH spectrum. Our results validate the coatings' effectiveness in biofouling prevention, aligning with goals for environmental sustainability and indicating their potential for wider application in desalination technologies. Further comprehensive evaluations, including extended time-based tests and cycle experiments, are recommended to substantiate long-term effectiveness and ease of biofilm removal under real-world scenarios.

### 3.4. Proposed antibiofouling mechanisms

It is important to note that the mechanisms proposed here are based on empirical observations and relevant literature rather than direct experimental validation within this study. This section provides a comprehensive discussion that synthesizes our findings and outlines biofouling control mechanisms correlated with the presented evidence.

#### 3.4.1. Surface hydrophilization: a key anti-adhesion strategy for initial biofilm prevention

The PDA-SP-cTA coating converts the PP surface from hydrophobic (WCA ~135.5°) to highly hydrophilic (WCA 23.3°, Fig. 3a). This transformation is hypothesized to hinder initial microbial attachment, potentially encourage the rapid dispersion of microorganisms in water, and reduce biofilm formation. In contrast, the uncoated hydrophobic PP surface might repel water, allowing microorganisms to remain in closer proximity, possibly facilitating their attachment. Even though the zeta potential of the coated surface becomes less negative at pH levels typically associated with microbial attachment (above pH 6.0, Fig. 3c), this change does not compromise its antifouling efficacy. Instead, the modification in surface charge, combined with increased hydrophilicity and the coating's diverse chemical functionality, establishes a comprehensive barrier against biofouling organism adhesion. This integrated approach, leveraging both hydrophilic properties and electrostatic repulsion, effectively enhances the surface's resistance to microbial colonization, as supported by previous studies [71,72].

#### 3.4.2. EPS disruption: a dual mechanism of microbicide action and anti-adhesion

The incorporation of citric acid-blended tannic acid (cTA) as a secondary coating significantly disrupts biofilm EPS, as detailed in Section 3.4. This disruption is believed to weaken the cohesive forces that hold the biofilm together, potentially facilitating its detachment from the surface. Additionally, the coated samples exhibit a simplified EPS composition, as presented in Section 3.5 (Fig. 9c–f, FEEM data), indicating its potential effect on the biofilm's structural integrity. The abundant phenolic hydroxyl content in TA is hypothesized to have a strong affinity for EPS components, suggesting its possible role in disrupting the biofilm matrix [24, 673]. This perceived disruption aligns with cTA's antimicrobial attributes. As the EPS matrix becomes less adhesive and possibly more disrupted, microorganisms within the biofilm do not adhere as strongly to the surface. This is consistent with the antiadhesive hypothesis, where the coating renders the surface less conducive to microbial attachment [71]. Moreover, a substantial 90 % reduction in carbohydrates and a 68 % decrease in proteins further underscore the profound impact of the coating on the biofilm's structural and compositional integrity, indicating a significant alteration in biofilm composition that may contribute to its diminished cohesiveness and stability. Thus, the impact on EPS can be viewed as a possible hybrid mechanism, reminiscent of both microbicides (influencing biofilm structure) and antiadhesives (potentially deterring initial attachment).

#### 3.4.3. Inhibition of active bacterial colonization: a pivotal antibiofouling mechanism of PDA-SP-cTA

The most noteworthy observation regarding the PDA-SP-cTA coating is the marked reduction in active bacterial gene copy numbers on the coated surface, as evidenced by RT-qPCR targeting 16S rRNA gene transcripts (Fig. 10b). This reduction, descending below the detection limit, highlights the effective inhibition of bacterial colonization, potentially reminiscent of direct microbicide-releasing strategies of applied coatings. Significant reductions in biomass thickness (94.1 %, Fig. 7 and Table 3) and ATP accumulation (73.6 %, Fig. 8c) further demonstrate the coating's substantial impact on reducing biofilm formation and microbial activity. Studies have shown that TA's antibacterial properties, possibly related to its phenolic hydroxyl groups, could interfere with bacterial cell membranes, enzymatic activities, and DNA replication and transcription processes [73]. Furthermore, the functionalization with citric acid is believed to enhance its microbicidal effects and potentially disrupt certain metabolic processes [74]. The coating's inhibitory effect on gene expression suggests interference with bacterial cell metabolism and gene regulation, making them less capable of adhering to and proliferating on the coated surface. This apparent downregulation of active bacterial genes could also impede biofilm establishment and growth. Moreover, the coating seems to inhibit the colonization of the dominant bacterial genus *Alteromonas*, well-known for its biofouling potential in seawater environments, as observed in uncoated controls (Fig. 10a). In summary, the PDA-SP-cTA coating appears to adopt a comprehensive antibiofouling strategy by leveraging anti-adhesion and microbicidal effects, as well as potential impacts on bacterial metabolism and gene expression, to combat biofouling effectively. While our findings suggest the intriguing possibility of interactions with bacterial communication mechanisms such as quorum sensing, further research is needed to explore these effects comprehensively. Together, these mechanisms may collaboratively reduce biomass accumulation, alter microbial communities, and enhance the coated surfaces' performance. By collectively addressing various biofilm developmental stages, this coating could effectively mitigate biofouling in seawater desalination systems. Owing to its holistic approach with minimal environmental impact, the PDA-SP-cTA coating emerges as a promising strategy to tackle biofouling challenges across diverse applications.

### 3.5. Future research directions

The current study elucidates the promising potential of the PDA-SP-cTA coating in mitigating biofouling in seawater desalination applications. Nevertheless, additional research is essential to comprehensively understand its capabilities and potential applications in industrial settings. The present study primarily concentrated on evaluating the coating's effectiveness in non-permeation modes, with an emphasis on feed channel pressure drop measurements. Future research should explore the coating's effectiveness, under permeation conditions, specifically examining variables such as the development of permeate flux and salt rejection. The applied coating inhibits biofouling by altering microbial by-product synthesis and tyrosine substances (Fig. 9c–f), resulting in loosely attached biofilms that could be easily removed by hydraulic cleaning. This alteration may enhance the penetration of cleaning chemicals into biofilms, potentially improving cleaning efficacy and reducing operational costs. Hence, future research should investigate the impact of PDA-SP-cTA coating on the efficiency of

advanced membrane cleaning and reapplication strategies, reinforcing its long-term applicability in biofouling management within seawater desalination systems. Such investigations may benefit from insights in related studies on materials science [75–77], which demonstrate how surface properties can be engineered to enhance environmental stability and performance. Future studies will include detailed evaluations of PDA-SP and cTA-SP coatings to elucidate their individual contributions and synergistic effects compared to the combined PDA-SP-cTA system, enabling a deeper understanding of their mechanisms and performance optimization. The PDA-SP-cTA coating exhibits excellent stability under operational pH conditions; however, future research will focus on optimizing its formulation to enhance stability in extreme alkaline environments (pH $>$ 12) by incorporating stabilizing agents or alternative polymer matrices. Furthermore, structured stability tests will be conducted to validate scalability and durability under operational stresses, including accelerated aging and exposure to diverse environmental conditions, to establish the coating's long-term performance over extended periods. This systematic approach will ensure the coating's readiness for real-world applications. Additionally, understanding the functional roles of specific genera, such as *Neptuniibacter*, in biofilm ecology and their interactions with extracellular polymeric substances (EPS) and quorum sensing pathways will provide deeper insights into the population selection effect of the coating, biofilm matrix stability, and system cleaning. Exploring the metabolic and ecological contributions of these genera, along with investigating molecular interactions between the coating and specific EPS components, such as tyrosine-like substances, could reveal mechanisms through which the coating disrupts biofilm structure, reduces microbial adhesion, and impacts microbial communication. These studies will also employ advanced spectroscopic and microscopic techniques to elucidate the stability and structural dynamics of the PDA-SP-cTA coating under operational conditions. Lastly, techno-economic implications of the PDA-SP-cTA coating should be explored, focusing on its potential to reduce cleaning and maintenance costs in operational settings. Evaluating the coating's stability and integrity after repeated fouling and cleaning cycles will be crucial to ensuring its durability and efficacy over time. Through a systematic investigation into these aspects, we can acquire a deeper understanding of the coating's influence on operational efficiency, microbial community dynamics, and biofilm matrix stability, thereby paving the way for its optimized application in industrial settings.

## 4. Conclusions

In this study, we have developed PDA-SP-cTA coating, an innovative solution with minimal environmental impact, for application in seawater desalination systems. Antibiofouling properties of the applied coating were evaluated through long-term biofouling tests in an MFS fed with UF-pretreated seawater and biodegradable nutrient dosing under flow conditions resembling those in industrial installations. Key findings are as follows: 1) PDA-SP-cTA coating significantly transforms surface properties, enhancing surface hydrophilicity, surface free energy, wettability, and surface charge. These modifications play a crucial role in hindering microbial adhesion and biofilm formation, thereby boosting the coating's antibiofouling effectiveness. 2) MFS systems coated both *in-situ* and *ex-situ* with PDA-SP-cTA exhibited a marked reduction in pressure drop increase, indicative of reduced biofouling compared to uncoated controls. 3) The coating demonstrated robust antiadhesive and antibacterial effects, as evidenced by notable reductions in biofilm thickness, total cell count (TCC), adenosine triphosphate (ATP), total organic carbon (TOC), and extracellular polymeric substances (EPS) levels. Furthermore, reductions in fluorescence intensities and the absence of specific EPS peaks in coated samples underscore the coating's effects on biofilm development and stability. 4) The surface coating also significantly impacted microbial diversity within the biofilms, leading to a decline in diversity, a shift in dominant genera and overall community structure, and a dramatic reduction in active bacterial gene copy numbers. This provides concrete evidence of the coating's effectiveness in inhibiting bacterial colonization. 5) Stability assessments of the PDA-SP-cTA coating highlighted its exceptional stability and durability, especially within the pH conditions commonly encountered in practical membrane-based applications, reinforcing its viability for long-term use. Furthermore, the coating's ability to alter microbial by-product synthesis leads to loosely attached biofilms, which could simplify hydraulic cleaning and enhance cleaning chemical penetration. This suggests a potential for improved cleaning efficacy and efficient reapplication strategies, indicating a promising direction for future research in biofouling management in seawater desalination systems.

## CRediT authorship contribution statement

**Krishnaveni Venkidusamy:** Writing – review & editing, Writing – original draft, Validation, Supervision, Software, Resources, Project administration, Methodology, Investigation, Formal analysis, Data curation, Conceptualization. **Laura Pulido-Beltran:** Writing – review & editing, Investigation. **Paulus J. Buijs:** Writing – review & editing, Methodology. **Daniel J. Miller:** Writing – review & editing, Methodology. **Johannes S. Vrouwenvelder:** Writing – review & editing, Project administration, Investigation, Funding acquisition. **Nadia M. Farhat:** Writing – review & editing, Project administration, Methodology.

## Declaration of competing interest

The authors declare that they have no known competing financial interests or personal relationships that could have appeared to influence the work reported in this paper.

## Acknowledgements

The research reported in this publication was supported by research translation funding from King Abdullah University of Science and Technology (KAUST) under grant REI/1/4455-01. We are deeply thankful to the editor and reviewers for their constructive feedback and insights, which have significantly refined and enhanced our manuscript. Their thorough assessments have enriched our understanding and greatly contributed to the development of this work.

## Appendix A. Supplementary data

Supplementary data to this article can be found online at https://doi.org/10.1016/j.memsci.2025.123809.

## Data availability

Data will be made available on request.

## References

[1] A. Matin, Z. Khan, S. Zaidi, M. Boyce, Biofouling in reverse osmosis membranes for seawater desalination: phenomena and prevention, Desalination 281 (2011) 1–16.
[2] H.-C. Flemming, Biofouling in water systems–cases, causes and countermeasures, Appl. Microbiol. Biotechnol. 59 (2002) 629–640.
[3] E. Bar-Zeev, U. Passow, S. Romero-Vargas Castrillón, M. Elimelech, Transparent exopolymer particles: from aquatic environments and engineered systems to membrane biofouling, Environmental Science & Technology 49 (2) (2015) 691–707.
[4] S.L. Percival, J.T. Walker, P.R. Hunter, Microbiological Aspects of Biofilms and Drinking Water, CRC press, 2000.
[5] M. Herzberg, M. Elimelech, Biofouling of reverse osmosis membranes: role of biofilm-enhanced osmotic pressure, J. Membr. Sci. 295 (1–2) (2007) 11–20.
[6] S. Sabella, R.P. Carney, V. Brunetti, M.A. Malvindi, N. Al-Juffali, G. Vecchio, S. M. Janes, O.M. Bakr, R. Cingolani, F. Stellacci, A general mechanism for intracellular toxicity of metal-containing nanoparticles, Nanoscale 6 (12) (2014) 7052–7061.
[7] J. Mansouri, S. Harrisson, V. Chen, Strategies for controlling biofouling in membrane filtration systems: challenges and opportunities, J. Mater. Chem. 20 (22) (2010) 4567–4586.

[8] W. Choi, M.G. Shin, C.H. Yoo, H. Park, Y.-I. Park, J.S. Lee, J.-H. Lee, Desalination membranes with ultralow biofouling via synergistic chemical and topological strategies, J. Membr. Sci. 626 (2021) 119212.
[9] W. Choi, M.G. Shin, G.W. Lee, D. Kim, C.H. Yoo, J.S. Lee, H.W. Jung, J.-H. Lee, Anisotropic biofouling behavior of sharkskin-patterned desalination membranes, J. Membr. Sci. 683 (2023) 121814.
[10] H. Lee, S.M. Dellatore, W.M. Miller, P.B. Messersmith, Mussel-inspired surface chemistry for multifunctional coatings, science 318 (5849) (2007) 426–430.
[11] D.J. Miller, P.A. Araújo, P.B. Correia, M.M. Ramsey, J.C. Kruithof, M.C. van Loosdrecht, B.D. Freeman, D.R. Paul, M. Whiteley, J.S. Vrouwenvelder, Short-term adhesion and long-term biofouling testing of polydopamine and poly (ethylene glycol) surface modifications of membranes and feed spacers for biofouling control, Water Res. 46 (12) (2012) 3737–3753.
[12] H. Kao, C.-C. Chen, Y.-R. Huang, Y.-H. Chu, A. Csik, S.-J. Ding, Metal ion-dependent tailored antibacterial activity and biological properties of polydopamine-coated titanium implants, Surf. Coating. Technol. 378 (2019) 124998.
[13] X. Zhang, Z. Wang, C.Y. Tang, J. Ma, M. Liu, M. Ping, M. Chen, Z. Wu, Modification of microfiltration membranes by alkoxysilane polycondensation induced quaternary ammonium compounds grafting for biofouling mitigation, J. Membr. Sci. 549 (2018) 165–172.
[14] Y. Zhang, F. Wang, Q. Huang, A.B. Patil, J. Hu, L. Fan, Y. Yang, H. Duan, X. Dong, C. Lin, Layer-by-layer immobilizing of polydopamine-assisted ε-polylysine and gum Arabic on titanium: tailoring of antibacterial and osteogenic properties, Mater. Sci. Eng. C 110 (2020) 110690.
[15] S. Goh, Y. Luan, X. Wang, H. Du, C. Chau, H. Schellhorn, J. Brash, H. Chen, Q. Fang, Polydopamine–polyethylene glycol–albumin antifouling coatings on multiple substrates, J. Mater. Chem. B 6 (6) (2018) 940–949.
[16] J. Cui, Y. Ju, K. Liang, H. Ejima, S. Lörcher, K.T. Gause, J.J. Richardson, F. Caruso, Nanoscale engineering of low-fouling surfaces through polydopamine immobilisation of zwitterionic peptides, Soft Matter 10 (15) (2014) 2656–2663.
[17] T.S. Sileika, D.G. Barrett, R. Zhang, K.H.A. Lau, P.B. Messersmith, Colorless multifunctional coatings inspired by polyphenols found in tea, chocolate, and wine, Angew. Chem. 125 (41) (2013) 10966–10970.
[18] J.A. Callow, M.E. Callow, Trends in the development of environmentally friendly fouling-resistant marine coatings, Nat. Commun. 2 (1) (2011) 244.
[19] F. Ponzio, J. Barthès, J. Bour, M. Michel, P. Bertani, J. Hemmerlé, M. d'Ischia, V. Ball, Oxidant control of polydopamine surface chemistry in acids: a mechanism-based entry to superhydrophilic-superoleophobic coatings, Chem. Mater. 28 (13) (2016) 4697–4705.
[20] J. Wang, H. Guo, X. Shi, Z. Yao, W. Qing, F. Liu, C.Y. Tang, Fast polydopamine coating on reverse osmosis membrane: process investigation and membrane performance study, J. Colloid Interface Sci. 535 (2019) 239–244.
[21] M. Li, L. Wu, C. Zhang, W. Chen, C. Liu, Hydrophilic and antifouling modification of PVDF membranes by one-step assembly of tannic acid and polyvinylpyrrolidone, Appl. Surf. Sci. 483 (2019) 967–978.
[22] Y. Du, W.Z. Qiu, Z.L. Wu, P.F. Ren, Q. Zheng, Z.K. Xu, Water-triggered self-Healing coatings of hydrogen-bonded complexes for high binding affinity and antioxidative property, Adv. Mater. Interfac. 3 (15) (2016) 1600167.
[23] W. Yan, M. Shi, C. Dong, L. Liu, C. Gao, Applications of tannic acid in membrane technologies: a review, Adv. Colloid Interface Sci. 284 (2020) 102267.
[24] H.M. Hegab, A. ElMekawy, T.G. Barclay, A. Michelmore, L. Zou, C.P. Saint, M. Ginic-Markovic, Single-step assembly of multifunctional poly (tannic acid)–graphene oxide coating to reduce biofouling of forward osmosis membranes, ACS applied materials & interfaces 8 (27) (2016) 17519–17528.
[25] P. Gawande, K. LoVetri, N. Yakandawala, T. Romeo, G. Zhanel, D. Cvitkovitch, S. Madhyastha, Antibiofilm activity of sodium bicarbonate, sodium metaperiodate and SDS combination against dental unit waterline-associated bacteria and yeast, J. Appl. Microbiol. 105 (4) (2008) 986–992.
[26] S. Mitrouli, A. Karabelas, N. Isaias, A. Al Rammah, Application of hydrophilic macromolecules on thin film composite polyamide membranes for performance restoration, Desalination 278 (1–3) (2011) 105–116.
[27] J. Vrouwenvelder, D.G. Von Der Schulenburg, J. Kruithof, M. Johns, M. Van Loosdrecht, Biofouling of spiral-wound nanofiltration and reverse osmosis membranes: a feed spacer problem, Water Res. 43 (3) (2009) 583–594.
[28] W. Lin, Y. Zhang, D. Li, X.-m. Wang, X. Huang, Roles and performance enhancement of feed spacer in spiral wound membrane modules for water treatment: a 20-year review on research evolvement, Water Res. 198 (2021) 117146.
[29] P.A. Araújo, D.J. Miller, P.B. Correia, M.C. van Loosdrecht, J.C. Kruithof, B. D. Freeman, D. Paul, J.S. Vrouwenvelder, Impact of feed spacer and membrane modification by hydrophilic, bactericidal and biocidal coating on biofouling control, Desalination 295 (2012) 1–10.
[30] A. Cihanoğlu, J.D. Schiffman, S. Alsoy Altinkaya, Biofouling-resistant ultrafiltration membranes via codeposition of dopamine and cetyltrimethylammonium bromide with retained size selectivity and water flux, ACS Appl. Mater. Interfaces 14 (33) (2022) 38116–38131.
[31] H. Basri, A. Ismail, M. Aziz, Microstructure and anti-adhesion properties of PES/TAP/Ag hybrid ultrafiltration membrane, Desalination 287 (2012) 71–77.
[32] H. Karkhanechi, R. Takagi, H. Matsuyama, Biofouling resistance of reverse osmosis membrane modified with polydopamine, Desalination 336 (2014) 87–96.
[33] Z. Liu, Y. Hu, Sustainable antibiofouling properties of thin film composite forward osmosis membrane with rechargeable silver nanoparticles loading, ACS Appl. Mater. Interfaces 8 (33) (2016) 21666–21673.
[34] D. Rice, A.C. Barrios, Z. Xiao, A. Bogler, E. Bar-Zeev, F. Perreault, Development of anti-biofouling feed spacers to improve performance of reverse osmosis modules, Water Res. 145 (2018) 599–607.
[35] J. Vrouwenvelder, S. Bakker, L. Wessels, J. Van Paassen, The membrane fouling simulator as a new tool for biofouling control of spiral-wound membranes, Desalination 204 (1–3) (2007) 170–174.
[36] J. Vrouwenvelder, J. Van Paassen, J. Van Agtmaal, M. Van Loosdrecht, J. Kruithof, A critical flux to avoid biofouling of spiral wound nanofiltration and reverse osmosis membranes: fact or fiction? J. Membr. Sci. 326 (1) (2009) 36–44.
[37] K. Drescher, Y. Shen, B.L. Bassler, H.A. Stone, Biofilm streamers cause catastrophic disruption of flow with consequences for environmental and medical systems, Proc. Natl. Acad. Sci. USA 110 (11) (2013) 4345–4350.
[38] N. Siebdrath, N. Farhat, W. Ding, J. Kruithof, J.S. Vrouwenvelder, Impact of membrane biofouling in the sequential development of performance indicators: feed channel pressure drop, permeability, and salt rejection, J. Membr. Sci. 585 (2019) 199–207.
[39] L. Neu, C.R. Proctor, J.-C. Walser, F. Hammes, Small-scale heterogeneity in drinking water biofilms, Front. Microbiol. 10 (2019) 2446.
[40] F.A. Hammes, T. Egli, New method for assimilable organic carbon determination using flow-cytometric enumeration and a natural microbial consortium as inoculum, Environmental Science & Technology 39 (9) (2005) 3289–3294.
[41] H. Liu, H.H. Fang, Extraction of extracellular polymeric substances (EPS) of sludges, J. Biotechnol. 95 (3) (2002) 249–256.
[42] S. Baghoth, S. Sharma, G. Amy, Tracking natural organic matter (NOM) in a drinking water treatment plant using fluorescence excitation–emission matrices and PARAFAC, Water Res. 45 (2) (2011) 797–809.
[43] S.F. Seyedpour, M. Dadashi Firouzjaei, A. Rahimpour, E. Zolghadr, A. Arabi Shamsabadi, P. Das, F. Akbari Afkhami, M. Sadrzadeh, A. Tiraferri, M. Elliott, Toward sustainable tackling of biofouling implications and improved performance of TFC FO membranes modified by Ag-MOF nanorods, ACS applied materials & interfaces 12 (34) (2020) 38285–38298.
[44] M. Pejman, M. Dadashi Firouzjaei, S. Aghapour Aktij, P. Das, E. Zolghadr, H. Jafarian, A. Arabi Shamsabadi, M. Elliott, M. Sadrzadeh, M. Sangermano, In situ Ag-MOF growth on pre-grafted zwitterions imparts outstanding antifouling properties to forward osmosis membranes, ACS applied materials & interfaces 12 (32) (2020) 36287–36300.
[45] M. Pejman, M.D. Firouzjaei, S.A. Aktij, E. Zolghadr, P. Das, M. Elliott, M. Sadrzadeh, M. Sangermano, A. Rahimpour, A. Tiraferri, Effective strategy for UV-mediated grafting of biocidal Ag-MOFs on polymeric membranes aimed at enhanced water ultrafiltration, Chem. Eng. J. 426 (2021) 130704.
[46] J.R. Cole, B. Chai, R.J. Farris, Q. Wang, A. Kulam-Syed-Mohideen, D.M. McGarrell, A. Bandela, E. Cardenas, G.M. Garrity, J.M. Tiedje, The ribosomal database project (RDP-II): introducing myRDP space and quality controlled public data, Nucleic acids research 35 (suppl_1) (2007) D169–D172.
[47] T. Iwasaki, Y. Tamai, M. Yamamoto, T. Taniguchi, K. Kishikawa, M. Kohri, Melanin precursor influence on structural colors from artificial melanin particles: PolyDOPA, polydopamine, and polynorepinephrine, Langmuir 34 (39) (2018) 11814–11821.
[48] F.S. Lameiras, A.L.d. Souza, V.A.R.d. Melo, E.H.M. Nunes, I.D. Braga, Measurement of the zeta potential of planar surfaces with a rotating disk, Mater. Res. 11 (2008) 217–219.
[49] B. Yu, J. Liu, S. Liu, F. Zhou, Pdop layer exhibiting zwitterionicity: a simple electrochemical interface for governing ion permeability, Chemical communications 46 (32) (2010) 5900–5902.
[50] A.K. Wardani, D. Ariono, Subagjo, I.G. Wenten, Hydrophilic modification of polypropylene ultrafiltration membrane by air-assisted polydopamine coating, Polym. Adv. Technol. 30 (4) (2019) 1148–1155.
[51] N.A. Che Lah, P. Murthy, M.N. Mohd Zubir, The physical and optical investigations of the tannic acid functionalised Cu-based oxide nanostructures, Sci. Rep. 12 (1) (2022) 9909.
[52] J. Jiang, L. Zhu, L. Zhu, H. Zhang, B. Zhu, Y. Xu, Antifouling and antimicrobial polymer membranes based on bioinspired polydopamine and strong hydrogen-bonded poly (N-vinyl pyrrolidone), ACS applied materials & interfaces 5 (24) (2013) 12895–12904.
[53] L. Pérez-Manríquez, P. Neelakanda, K.-V. Peinemann, Tannin-based thin-film composite membranes for solvent nanofiltration, J. Membr. Sci. 541 (2017) 137–142.
[54] C. Dreszer, H.-C. Flemming, A. Zwijnenburg, J. Kruithof, J.S. Vrouwenvelder, Impact of biofilm accumulation on transmembrane and feed channel pressure drop: effects of crossflow velocity, feed spacer and biodegradable nutrient, Water Res. 50 (2014) 200–211.
[55] L. Javier, N.M. Farhat, J.S. Vrouwenvelder, Enhanced hydraulic cleanability of biofilms developed under a low phosphorus concentration in reverse osmosis membrane systems, Water Res. X 10 (2021) 100085.
[56] I. Biswas, M. Sadrzadeh, A. Kumar, Impact of bacterial streamers on biofouling of microfluidic filtration systems, Biomicrofluidics 12 (4) (2018).
[57] J. Zhu, C.B. Thompson, Metabolic regulation of cell growth and proliferation, Nat. Rev. Mol. Cell Biol. 20 (7) (2019) 436–450.
[58] I. Singh, G. Dhawan, S. Gupta, P. Kumar, Recent advances in a polydopamine-mediated antimicrobial adhesion system, Front. Microbiol. 11 (2021) 607099.
[59] D.L. Zhao, Q. Zhao, H. Lin, S.B. Chen, T.-S. Chung, Pressure-assisted polydopamine modification of thin-film composite reverse osmosis membranes for enhanced desalination and antifouling performance, Desalination 530 (2022) 115671.
[60] H.-C. Flemming, G. Schaule, T. Griebe, J. Schmitt, A. Tamachkiarowa, Biofouling—the Achilles heel of membrane processes, Desalination 113 (2–3) (1997) 215–225.

[61] L. Huang, Y. Jin, D. Zhou, L. Liu, S. Huang, Y. Zhao, Y. Chen, A review of the role of extracellular polymeric substances (EPS) in wastewater treatment systems, Int. J. Environ. Res. Publ. Health 19 (19) (2022) 12191.
[62] P.H. Santschi, C. Xu, K.A. Schwehr, P. Lin, L. Sun, W.-C. Chin, M. Kamalanathan, H. P. Bacosa, A. Quigg, Can the protein/carbohydrate (P/C) ratio of exopolymeric substances (EPS) be used as a proxy for their 'stickiness' and aggregation propensity? Mar. Chem. 218 (2020) 103734.
[63] T. Sushmitha, M. Rajeev, P. Sriyutha Murthy, S. Ganesh, S.R. Toleti, S. Karutha Pandian, Bacterial community structure of early-stage biofilms is dictated by temporal succession rather than substrate types in the southern coastal seawater of India, PLoS One 16 (9) (2021) e0257961.
[64] M. Zhang, S. Jiang, D. Tanuwidjaja, N. Voutchkov, E.M. Hoek, B. Cai, Composition and variability of biofouling organisms in seawater reverse osmosis desalination plants, Appl. Environ. Microbiol. 77 (13) (2011) 4390–4398.
[65] B. Grasland, J. Mitalane, R. Briandet, E. Quemener, T. Meylheuc, I. Linossier, K. Vallee-Rehel, D. Haras, Bacterial biofilm in seawater: cell surface properties of early-attached marine bacteria, Biofouling 19 (5) (2003) 307–313.
[66] C.d.O. Manes, C. Barbe, N. West, S. Rapenne, P. Lebaron, Impact of seawater-quality and water treatment procedures on the active bacterial assemblages at two desalination sites, Environmental science & technology 45 (14) (2011) 5943–5951.
[67] H. Dang, C.R. Lovell, Bacterial primary colonization and early succession on surfaces in marine waters as determined by amplified rRNA gene restriction analysis and sequence analysis of 16S rRNA genes, Appl. Environ. Microbiol. 66 (2) (2000) 467–475.
[68] N.P. Boks, W. Norde, H.C. van der Mei, H.J. Busscher, Forces involved in bacterial adhesion to hydrophilic and hydrophobic surfaces, Microbiology 154 (10) (2008) 3122–3133.
[69] S. Zheng, M. Bawazir, A. Dhall, H.-E. Kim, L. He, J. Heo, G. Hwang, Implication of surface properties, bacterial motility, and hydrodynamic conditions on bacterial surface sensing and their initial adhesion, Front. Bioeng. Biotechnol. 9 (2021) 643722.
[70] H.T. Nguyen, W. Choi, E.-J. Kim, K. Cho, Microbial community niches on microplastics and prioritized environmental factors under various urban riverine conditions, Sci. Total Environ. 849 (2022) 157781.
[71] A. Uneputty, A. Dávila-Lezama, D. Garibo, A. Oknianska, N. Bogdanchikova, J. Hernández-Sánchez, A. Susarrey-Arce, Strategies applied to modify structured and smooth surfaces: a step closer to reduce bacterial adhesion and biofilm formation, Colloid and Interface Science Communications 46 (2022) 100560.
[72] P. Singha, J. Locklin, H. Handa, A review of the recent advances in antimicrobial coatings for urinary catheters, Acta Biomater. 50 (2017) 20–40.
[73] W. Jing, C. Xiaolan, C. Yu, Q. Feng, Y. Haifeng, Pharmacological effects and mechanisms of tannic acid, Biomed. Pharmacother. 154 (2022) 113561.
[74] E. Gungormus, S.A. Altinkaya, Facile fabrication of Anti-biofouling polyaniline ultrafiltration membrane by green citric acid doping process, Separation and Purification Technology 279 (2021) 119756.
[75] M. Zhu, S. Yang, D. Wang, J. Hogan, M. Sadrzadeh, CTAC-assisted monoclinic BiVO4 with oxygen defects for efficient photocatalytic performances: a combined experimental and DFT study, J. Alloys Compd. 990 (2024) 174404.
[76] M. Zhu, Y. Liu, A. Rahimpour, Y. Liu, M. Sadrzadeh, Fabrication of fluorine-free pH-responsive functionalized mesh via thiol-ene click chemistry for oil-water separation, Surf. Coating. Technol. 470 (2023) 129792.
[77] M. Zhu, Y. Liu, M. Chen, M. Sadrzadeh, Z. Xu, D. Gan, Z. Huang, L. Ma, B. Yang, Y. Zhou, Robust superhydrophilic and underwater superoleophobic membrane optimized by Cu doping modified metal-organic frameworks for oil-water separation and water purification, J. Membr. Sci. 640 (2021) 119755.